Lattice computation of the decay constants of B and D mesons

Claude W. Bernard
Department of Physics, Washington University, St. Louis, Missouri 63130

James N. Labrenz
Department of Physics FM-15, University of Washington, Seattle, Washington 98195

Amarjit Soni
Department of Physics, Brookhaven National Laboratory, Upton, New York 11973

(Received 1 July 1993)

A lattice calculation of the pseudoscalar decay constant of heavy-light mesons is reported. Results are obtained (in the quenched approximation) from lattices at $\beta=6.3$ through a procedure that interpolates between the static approximation of Eichten and the conventional ("heavy" Wilson fermion) method. The previously observed discrepancy between these two approaches has been resolved: we find the scaling quantity $f\sqrt{M}$ to be significantly smaller than previous calculations had indicated (e.g., at $\beta=6.0$); in addition, we discuss a modification which is required in normalizing the conventional amplitude to correct for large-am lattice errors. This change guarantees that $f\sqrt{M}$ will smoothly approach its value in the static limit. From the numerical interpolation of the static and intermediate-mass results, we find, in units of MeV, $f_B=187(10)\pm34\pm15$, $f_{B_s}=207(9)\pm34\pm22$, $f_D=208(9)\pm35\pm12$, and $f_{D_s}=230(7)\pm30\pm18$, where the first error is statistical and the second two are estimates of systematics due to (1) fitting and large-am effects and (2) scaling. The ratios are better determined: f_D/f_{D_s}, f_B/f_{B_s}, f_B/f_D, and f_{B_s}/f_{D_s} are all 0.90 within a total error of less than 0.05. The purely static values are $f_B^{\rm stat}=235(20)\pm21$ MeV, $f_{B_s}^{\rm stat}=259(19)\pm19$ MeV, and $f_B^{\rm stat}/f_{B_s}^{\rm stat}=0.90(2)\pm0.02$. Finally, using lattices at $\beta=6.3$, $\beta=6.0$, and $\beta=5.7$ and extrapolating to the limit of zero lattice spacing, we have computed $f_K/f_\pi=1.08\pm0.03\pm0.08$ in the quenched approximation, where the first error includes statistical and fitting errors, and the second is an estimate of the error in extrapolation to the continuum limit.

PACS number(s): 12.38.Gc, 11.15.Ha, 14.40.Lb, 14.40.Nd

I. INTRODUCTION

The calculation of transition amplitudes for heavy-light mesons has recently been a topic of great interest, from both a theoretical and a phenomenological standpoint. Theoretically, the static limit, in which the mass of the heavy quark is taken *a priori* to infinity, has been used to define an effective theory for quantum chromodynamics (QCD) which has additional flavor and spin symmetries [1,2]. In continuum calculations, these symmetries have been used to compute relations among various heavy-meson form factors. On the lattice, the symmetry limit is equally well defined: the heavy quark is replaced with a static color source, so only the light quark degree of freedom is subject to the usual constraint imposed by the lattice cutoff, $m_q \ll 1/a$, where m_q denotes the quark mass and a the grid spacing. This approach, introduced in [1], provides a method for explicit calculation of heavy-light amplitudes, such as the static limit of the pseudoscalar decay constants f_{Qq}. (We use Q to denote a heavy quark, such as b or c, and q a light quark, u, d, or s.)

From the point of view of phenomenology, a great deal of emphasis has in particular been placed on f_B. Notwithstanding the physical process through which it is defined (i.e., the leptonic decay of the B), which may in the future be accessible to experiment, f_B already plays an important role in standard model (SM) physics. As a characteristic example, consider the usual parametrization of the B-$\bar{B}$ mixing parameter, $x_{bd}\equiv\Delta M/\Gamma$. From the evaluation of the top-quark-dominated box diagram, one finds

$$x_{bd}\sim h(m_t)|V_{td}|^2 f_B^2 B_B \ , \tag{1.1}$$

where h is a rapidly increasing function of m_t, the top quark mass, V_{td} is a Cabibbo-Kobayashi-Maskawa (CKM) matrix element, and B_B is the so-called "B parameter" relating the full matrix element of the weak interaction Hamiltonian to its value in the vacuum insertion approximation [3]. The measurement of x_{bd} only determines the fundamental SM parameter V_{td} if f_B and B_B are known.

With respect to lattice QCD, there are essential (technical) differences which affect the calculation of these two quantities. Because it is computed as a dimensionless ratio, B_B is more amenable than f_B to the "conventional" method (i.e., using one light and one heavy Wilson quark). These calculations have indicated that vacuum insertion (i.e., $B_B\simeq1$) becomes a fairly good approxima-

tion at moderately heavy quark masses; the extrapolation of this result to the B meson is then straightforward [4,5]. The large-am normalization effects (see Secs. II D and II E) cancel in the ratio that defines B_B. For f_B such leading-order lattice errors will no longer cancel. Nonetheless, a similar strategy is possible in principle: one may simulate moderately heavy mesons where large-am_Q lattice errors are presumed to be small and look for asymptotic behavior in f. Indeed, in the static limit one has [1]

$$\phi \equiv f\sqrt{M} \underset{M\to\infty}{\longrightarrow} \text{const} \tag{1.2}$$

(up to corrections logarithmic in m_Q, the heavy-quark mass [2]). This may then provide a guide for extrapolating to the physical B meson [4–6].

In early calculations at moderate couplings (i.e., $\beta=5.7$, 5.9, and 6.0), it became evident that there was a significant discrepancy between the two approaches: f_B^{stat}, the decay constant computed in the static limit, was much larger than extrapolations from lighter masses indicated it should be [7–10]. It was difficult to know whether one or both of the methods suffered from large systematic errors, and because of this, interpolating between them, as a way of computing the finite-mass corrections to the scaling law (1.2), was certainly unreliable. In this paper we demonstrate the elimination of this discrepancy; thus we are able to interpolate smoothly between the intermediate-mass regime of the conventional calculation and the infinite-mass limit of the static one in order to compute physical amplitudes. The discrepancy has disappeared as a result of two essential differences. First, as compared to the results mentioned above, we find a smaller static result for ϕ from our computation at $\beta=6.3$. Second, we find that "large-am_Q" errors must be corrected for, even when only "moderately" heavy quarks are used, in order for the conventional amplitude to smoothly approach the correct static limit as the heavy-quark mass m_Q is increased.

This paper is organized as follows. In Sec. II we discuss some essential details of the calculation, emphasizing in particular how the correction of large-am_Q errors in the conventional method ensures that it (approximately) match, in the limit $m_Q\to\infty$, with the static result. The numerical techniques used throughout the calculation are described in Sec. III. In Sec. IV, we discuss the details of the analysis and present results for f_B, f_{B_s}, f_D, f_{D_s} and their jackknifed ratios, including estimates for various systematic errors. We summarize and make concluding remarks in Sec. V. Some of these results have been reported previously [11].

II. LATTICE DECAY CONSTANTS

A. The conventional method

The decay constant f_P for a pseudoscalar P (with arbitrary quark masses m_Q and m_q) is defined as the vacuum to single-particle matrix element of the axial-vector current:

$$\langle 0|A_\mu^{\text{cont}}(x)|P(\mathbf{p})\rangle = -if_P p_\mu e^{-ip\cdot x} , \tag{2.1}$$

where our normalization is such that $f_\pi^{\text{expt}}=132$ MeV. We compute f_P through the evaluation of two lattice correlation functions:

$$G_A(t-t_0)\equiv\sum_{\mathbf{x}}\langle 0|TA_0(\mathbf{x},t)\chi^\dagger(\mathbf{0},t_0)|0\rangle , \tag{2.2a}$$

and

$$G_B(t-t_0)\equiv\sum_{\mathbf{x}}\langle 0|T\chi(\mathbf{x},t)\chi^\dagger(\mathbf{0},t_0)|0\rangle . \tag{2.2b}$$

For the conventional calculation, we write A_μ, the lattice axial vector current, and χ, the pseudoscalar interpolating operator, as

$$A_\mu(x)=\bar{q}(x)\gamma_\mu\gamma_5 Q(x) , \tag{2.3a}$$

$$\chi(x)=\bar{q}(x)\gamma_5 Q(x) , \tag{2.3b}$$

where the fields $q(x)$ and $Q(x)$ are the "light" and "heavy" fermionic fields, respectively, defined via the standard Wilson action with quark hopping parameters κ_q and κ_Q. In this section, we choose χ to be the local operator given above, primarily to simplify the discussion of various normalization issues which are independent of the source type. For the actual computations, we have used both local sources and extended (or "smeared") sources in a fixed gauge, the latter as a means of improving the numerical precision of the results. The specific techniques will be discussed in Sec. III; their actual implementation in the computations, in Sec. IV.

Evaluating the Wick contractions of the quark fields, Eqs. (2.2) are written as a configuration average of contracted light- and heavy-quark propagators S_q and S_Q. For example,

$$G_A(t)=-\left\langle\sum_{\mathbf{x}}\text{Tr}[S_q^\dagger(\mathbf{x},t;\mathbf{0},0;U)\times\gamma_0 S_Q(\mathbf{x},t;\mathbf{0},0;U)]\right\rangle_{\{U\}} . \tag{2.4}$$

The essential formula for the calculation follows from the insertion of a complete set of states between the interpolating operators in Eq. (2.2). Excited states are exponentially damped, and thus at large times (with $t_0\equiv 0$) we obtain

$$G_A(t)\underset{|t|\to\infty}{\sim}\frac{\langle 0|A_0|P\rangle\langle P|\chi^\dagger|0\rangle}{2M_P}e^{-aM_P|t|} \equiv\zeta_A e^{-aM_P|t|} , \tag{2.5a}$$

and

$$G_B(t)\underset{|t|\to\infty}{\sim}\frac{\langle 0|\chi|P\rangle\langle P|\chi^\dagger|0\rangle}{2M_P}e^{-aM_P|t|} \equiv\zeta_B e^{-aM_P|t|} . \tag{2.5b}$$

From (2.1) and (2.5), f_P is given by

$$\phi_P=f_P\sqrt{M_P}=C_A\left[\frac{2\zeta_A^2}{\zeta_B}\right]^{1/2}a^{-3/2} . \tag{2.6}$$

C_A is the normalization constant between the continuum current $A_\mu^{\rm cont}$ and its lattice counterpart A_μ. Although we have illustrated the computation of the correlators using the conventional method [i.e., Eq. (2.4)], Eq. (2.6), with suitable modifications to the constant C_A, holds also for the static-quark approach. We discuss the details of the static and conventional normalizations in the following sections.

B. The static effective theory

In this section we discuss the implementation of the static-quark method, emphasizing in particular how the lattice calculation is normalized to obtain continuum physics. We begin by writing the discretized effective action [12]

$$\mathcal{S}^{(0)}=\sum_x \bar{h}(x)\left[\frac{1+\gamma_0}{2}\right][h(x)-U_0^\dagger(x-\hat{0})h(x-\hat{0})]\ , \tag{2.7}$$

where $h(x)$ denotes the static *quark* (as opposed to antiquark) field at site x. In the particle's rest frame the lower two components of h vanish, a condition enforced by the constraint equation [13]

$$\gamma_0 h = h\ . \tag{2.8}$$

The quark and antiquark are decoupled; we omit the analogous formulas pertaining to the latter.

Renormalization requires the addition of a mass counterterm $a\delta m\bar{h}h$ to the action (2.7), yielding [12]

$$\mathcal{S}^{(\delta m)}=\sum_{x,y}\bar{h}(x)S_h^{-1}(x,y)h(y)\ , \tag{2.9}$$

where

$$S_h^{-1}(x,y)=(1+a\delta m)\left[\frac{1+\gamma_0}{2}\right]\times\left[\delta^4_{x,y}-\frac{1}{1+a\delta m}U_0^\dagger(y)\delta^4_{x-\hat{0},y}\right]\ . \tag{2.10}$$

The matrix S_h^{-1} is then inverted for the static-quark propagator in the background gauge configuration U:

$$S_h(x,y)=\frac{1}{1+a\delta m}e^{-\ln(1+a\delta m)(t_x-t_y)}\theta(t_x-t_y)\delta^3_{\mathbf{x},\mathbf{y}}\left[\frac{1+\gamma_0}{2}\right]\{U_0^\dagger(\mathbf{y},t_y)U_0^\dagger(\mathbf{y},t_y+1)U_0^\dagger(\mathbf{y},t_y+2)\cdots U_0^\dagger(\mathbf{y},t_x-1)\}$$
$$\equiv\frac{1}{1+a\delta m}e^{-\ln(1+a\delta m)(t_x-t_y)}S_h^{(0)}(x,y)\ . \tag{2.11}$$

We denote quantities computed in the static approximation with a careted version of the notation used in Sec. II A. The static-light current $\hat{A}_\mu$ and the interpolating operator $\hat{\chi}$ are defined via the substitution $Q(x)\to h(x)$ in Eqs. (2.3), and the construction of the correlation functions $\hat{G}_A$ and $\hat{G}_B$ is analogous to Eqs. (2.2). To compute the correlators, the heavy-quark propagator is simply replaced by the static one, as given by (2.11). The calculation of $\hat{\phi}$ then follows according to Eqs. (2.5) and (2.6).

However, since the heavy-quark mass has been formally removed from the theory the correlation functions $\hat{G}_A$ and $\hat{G}_B$ no longer fall exponentially with the meson mass M_P, as in Eqs. (2.5), but instead with the bare and divergent "binding energy," $\mathcal{E}_0=M_P-m_Q$. In the Wilson case, the bare mass, or its equivalent in terms of the hopping parameter, appears in the action, so the mass divergence can be absorbed in the usual way. Here, i.e., in Eq. (2.7), the bare mass is absent—it has been absorbed in the definition of the field—and the counterterm must be explicitly added. In the literature this issue has been addressed concurrently with the calculation of $\hat{C}_A$, the normalization constant for the static-light axial current ($A_\mu^{\rm cont}=\hat{C}_A\hat{A}_\mu$), because that calculation must include in some way the mass renormalization $a\delta m$, which enters into the overall normalization of the heavy-quark propagator through Eq. (2.11).

Two groups (Boucaud *et al.* [14] and Eichten and Hill [15,12]) have calculated the renormalization constant which matches $\hat{A}_\mu$ to the full axial vector current of QCD to one loop in perturbation theory. We write this constant as the product $\hat{Z}_A C(a,m)$, where

$$C(a,m)=1+\frac{g^2C_F}{16\pi^2}[\tfrac{3}{2}\ln(a^2m^2)]\ , \tag{2.12}$$

and

$$\hat{Z}_A=1-\frac{g^2C_F}{16\pi^2}(J+2)\ , \tag{2.13}$$

where $C_F=\frac{4}{3}$ for the case of SU(3). For reasons which will be made clear below, we have split off into $C(a,m)$ the dependence on the heavy quark mass. Before accounting for the effect of mass renormalization, i.e., the term $1/(1+a\delta m)$ in Eq. (2.11), Eichten and Hill find [12] $J=30.35$. (After including mass renormalization, one gets $J=20.38$—see below.) They propose two methods for the complete matching.

In order to illustrate their approach, let us consider the point-source correlator[1]

$$\hat{G}_A(t)=\sum_{\mathbf{x}}\langle 0|\hat{A}_0(\mathbf{x},t),\hat{\chi}^\dagger(\mathbf{0},0)|0\rangle\ . \tag{2.14}$$

Again specifying $t>0$, we obtain

[1]In practice we always use a smeared interpolating operator for the static computations. The result of this discussion, however, is unaffected by this modification; here we use a point source for simplicity.

$$\hat{G}_A(t)=\left\langle \sum_{\mathbf{x}} \mathrm{Tr}[\gamma_0 S_h(x,0)\gamma_5 S_q(0,x)\gamma_5] \right\rangle_{\{U\}}$$
$$=\left\langle \sum_{\mathbf{x}} \delta^3_{\mathbf{x},0}\mathrm{Tr}\left[\mathcal{P}(t,0)\left[\frac{1+\gamma_0}{2}\right]S_q^\dagger(x,0)\right]\right\rangle_{\{U\}} \frac{1}{1+a\delta m} e^{-\ln(1+a\delta m)t}$$
$$\equiv \hat{G}_A^{(0)}(t)e^{-a\delta\mathcal{E}}e^{-a\delta\mathcal{E}t} , \tag{2.15}$$

where $\hat{G}_A^{(0)}(t)$ is the "bare" correlator which follows from the action (2.7), $\mathcal{P}(t,0)$ stands for the appropriate product of link matrices, as given in (2.11), and we have defined $a\delta\mathcal{E}=\ln(1+a\delta m)$. The two scenarios of Ref. [12] are the following.

Method 1. Parametrize (i.e., fit) $\hat{G}_A^{(0)}$ as $\hat{\xi}_A e^{-a\mathcal{E}_0 t}$. Then (2.15) is written as

$$\hat{G}_A(t)=(\hat{\xi}_A e^{-a\delta\mathcal{E}})e^{-a(\mathcal{E}_0+\delta\mathcal{E})t} ,$$

which shows explicitly how the linear divergence in $\mathcal{E}_0$ is removed to define the physical binding energy, $\mathcal{E}=\mathcal{E}_0+\delta\mathcal{E}\simeq\mathcal{E}_0+\delta m$. But in this case, the residue of $\hat{G}_A$ includes a correction to the bare fitted value. In other words, we should use $\hat{\xi}_A^{(1)}$ instead of $\hat{\xi}_A$ in the static analog of Eq. (2.6), where

$$\hat{\xi}_A^{(1)}=\hat{\xi}_A e^{-a\delta\mathcal{E}} . \tag{2.16}$$

Method 2. Parametrize $\hat{G}_A^{(0)}$ as $\hat{\xi}_A^{(2)}e^{-a\mathcal{E}_0(t+1)}$ so that (2.15) is instead written as

$$\hat{G}_A(t)=\hat{\xi}_A^{(2)}e^{-a(\mathcal{E}_0+\delta\mathcal{E})(t+1)} .$$

The physical binding energy emerges as before, and it is trivial to see that the residue now satisfies the equation

$$\hat{\xi}_A^{(2)}=\hat{\xi}_A e^{a\mathcal{E}_0}=\hat{\xi}_A e^{a(\mathcal{E}-\delta\mathcal{E})}=\hat{\xi}_A^{(1)}e^{a\mathcal{E}} . \tag{2.17}$$

(Note that $\hat{\xi}_A$ is still *defined* by the fit of method 1.)

Equation (2.17) demonstrates explicitly that the two methods differ at finite a. Method 2, chosen in Ref. [12], appears to us to be an unnatural choice which introduces $O(a)$ terms in order to accommodate a suggestive form of the propagator. Method 1, however, simply parallels the standard procedure for Wilson quarks. This can be seen as follows. A rescaling of the static field in the action (2.9), given by

$$h\rightarrow(1+a\delta m)^{-1/2}h , \tag{2.18}$$

normalizes the diagonal term of (2.10) to unity, an analogous procedure to the quark field rescaling

$$\psi\rightarrow\left[\frac{1}{2\kappa}\right]^{-1/2}\psi \tag{2.19}$$

which leads to the standard form of the Wilson action. In the latter case, quark-mass renormalization is achieved through tuning the hopping parameter κ such that the correct physical spectrum is reproduced, and a factor $\sqrt{2\kappa}$ for each quark field is ultimately replaced in physical amplitudes. If the physical binding energy $\mathcal{E}$ of the heavy-light state were experimentally measurable, a similar tuning procedure, instead of a perturbative calculation, could be used to determine $a\delta m$ in the static case. Either with tuning or with perturbation theory, the rescaling of the static field(s) in physical amplitudes following (2.18) is equivalent to method 1.

Therefore, $\hat{\xi}_A$ and $\hat{\xi}_B$ will denote the residues computed from a fit to the bare correlators; we use them in the static analog of Eq. (2.6). The remaining factor of $e^{-a\delta\mathcal{E}/2}\simeq 1-a\delta m/2$ is absorbed into the perturbative renormalization of the static-light axial vector current. From [12] we find

$$a\delta m=-\frac{g^2C_F}{16\pi^2}19.95 \tag{2.20}$$

and thus obtain

$$\hat{Z}_A=1-\frac{g^2C_F}{16\pi^2}22.38 . \tag{2.21}$$

[A rigorous treatment of the ambiguity discussed above has been given by Boucaud *et al.* [16], and they show that method 2 is in fact inconsistent with an $O(a)$ improvement of the light-quark action. Equation (2.21) is in agreement with their result.] Including the factor $\sqrt{2\kappa}$ for the light quark, we thus obtain

$$\hat{C}_A=\sqrt{2\kappa_q}\hat{Z}_A C(a,m_Q) . \tag{2.22}$$

C. The naive large-mass limit

The conventional normalization for the light meson decay constants is given by

$$C_A=Z_A\sqrt{2\kappa_Q}\sqrt{2\kappa_q} , \tag{2.23}$$

where Z_A is the perturbative renormalization of the lattice axial current [17],

$$Z_A=1-0.133g^2 , \tag{2.24}$$

and the factors of $\sqrt{2\kappa}$ undo the initial rescaling of the Wilson quark fields, indicated by Eq. (2.19). Since we wish to interpolate between the static and conventional methods, it is instructive to consider the latter in the naive limit $m_Q\rightarrow\infty$ (i.e., $\kappa_Q\rightarrow 0$). In this case the propagator can be approximated by the leading term in the hopping-parameter expansion:

$$S_Q(x,0)\underset{\kappa_Q\rightarrow 0}{\sim}(2\kappa_Q)^t\delta^3_{\mathbf{x},0}\theta(t)\left[\frac{1+\gamma_0}{2}\right]\mathcal{P}(t,0)$$
$$=e^{-\ln(1/2\kappa_Q)t}S_h^{(0)}(x,0) . \tag{2.25}$$

Using (2.25) to compute the bare (unnormalized) heavy-light correlation function, we obtain identically the bare

static-light result, but with a heavy-quark rest mass contributing to the inverse correlation length:

$$G_A \sim \hat{\xi}_A e^{-(aM_P)t}, \tag{2.26a}$$

$$G_B \sim \hat{\xi}_B e^{-(aM_P)t}, \tag{2.26b}$$

and

$$aM_P \underset{\kappa_Q \to 0}{\sim} \ln\left[\frac{1}{2\kappa_Q}\right]. \tag{2.27}$$

Therefore, using (2.23) and (2.22), one finds the limiting expression

$$\phi_P \underset{\kappa_Q \to 0}{\sim} \hat{\phi}_P e^{-aM_P/2}[1+O(\alpha_s)], \tag{2.28}$$

where the factor of $e^{-aM_P/2}$ just comes from the $\sqrt{2\kappa_Q}$ in (2.23). Thus, when κ_Q is pushed to absurdly small values, a pure lattice artifact [the factor $e^{-aM_P/2}$ in (2.28)] will dominate in the heavy-light amplitude.

D. The leading-order large-*am* correction

Equation (2.28) demonstrates that the systematic lattice error when $am_Q \gg 1$ can be removed in the static limit by a trivial redefinition of the normalization constant C_A. This modification can be formulated in terms of a large-*am* corrected normalization for the Wilson quark. In order to derive it, let us first consider the free theory. Computing the spatially summed propagator both from the Wilson action (with $U=1$) and in the continuum, one finds the normalization equation

$$2\kappa e^{am} \sum_{\mathbf{x}} \langle 0|\psi(x)\bar{\psi}(0)|0\rangle^{\text{latt}} = \int d^3\mathbf{x} \langle 0|\psi(x)\bar{\psi}(0)|0\rangle^{\text{cont}}, \tag{2.29}$$

where

$$am = \ln\left[1+\frac{1}{2\kappa}-\frac{1}{2\kappa_c^{(0)}}\right]; \quad \kappa_c^{(0)} = \frac{1}{8}. \tag{2.30}$$

Based on this relation, or on equivalent arguments, a change in the tree-level Wilson quark normalization factor of

$$\sqrt{2\kappa} \to \sqrt{2\kappa e^{am}} \tag{2.31}$$

has been suggested [18–20]. Note that Eq. (2.29) is valid for arbitrary *am*, but that it is a zero-momentum (or static) relation. In the regime where $am \ll 1$, the zero-momentum projection is irrelevant, because the usual factor of $\sqrt{2\kappa}$ is recovered. Conversely, since a typical simulation of light hadrons requires that $a^{-1} \gg \Lambda_{\text{QCD}}$, the condition $am \gtrsim 1$ implies that $m_Q \gg \Lambda_{\text{QCD}}$, and therefore that the heavy-quark dynamics in this regime are nonrelativistic. Within the context of a nonrelativistic expansion of the heavy-quark propagator, we thus refer to the factor e^{am} in (2.31) as the large-*am* correction for the leading-order term. It guarantees a smooth transition between the light- and static-quark regimes. In the remaining part of this section, we discuss the inclusion of interactions, and in the following section we examine the large-*am* lattice errors in the next-to-leading terms of the quark propagator in this limit.

A full one-loop correction to (2.29) for arbitrary *am* has not been computed. However, in lattice perturbation theory, the primary contribution to a variety of short-distance-dominated quantities is produced by tadpole graphs. Lepage and Mackenzie have demonstrated that a mean-field approach can be used to improve the matching between lattice operators and their continuum counterparts; in a rough sense, this technique sums tadpole contributions to all orders in α_s [21]. (The sense is rough because "summing the tadpoles" is not a gauge-invariant procedure beyond leading order, but the mean field approach of [21] is gauge invariant.) The "tadpole correction" is easily made to the free-theory equation (2.29) because it is independent of the quark momentum. In the mean-field language, one substitutes the link matrices in the Wilson action with the mean value u_0. Computationally, the theory is then equivalent to the free one with a hopping parameter shifted by

$$\kappa \to u_0 \kappa. \tag{2.32}$$

Thus tadpole improvement of the leading-order correction "e^{am}" is given by $am \to a\tilde{m}$, where, from (2.30),

$$a\tilde{m} = \ln\left[\frac{1}{2u_0\kappa}-3\right]. \tag{2.33}$$

Several defining relations for the quantity u_0 are possible; all give similar results, either when computed nonperturbatively or to one loop in perturbation theory using a boosted coupling [21]. We use the definition

$$u_0 = \frac{\kappa_c^{(0)}}{\kappa_c} = \frac{1}{8\kappa_c}, \tag{2.34}$$

where κ_c is the critical hopping parameter, as determined by the extrapolation to zero pion mass.

Now let us return to C_A, the normalization constant for the axial current. The tadpole-improved large-*am* correction requires the substitution for the quark-line normalization factor, $\sqrt{2\kappa} \to \sqrt{2u_0\kappa e^{a\tilde{m}}}$. However, if used in Eq. (2.23) as it stands, this will double count the leading tadpole perturbative correction, which already contributes to Z_A. Let us write the perturbative renormalization in the form

$$Z_A = Z_1 Z_{2a}^{-1} Z_{2b}^{-1},$$

where Z_1 is the vertex correction, Z_{2a} is the wave-function renormalization from the continuumlike self-energy graph, and Z_{2b} is the wave-function renormalization from the tadpole. It is easily verified that to one loop in perturbation theory, u_0, the tadpole contribution to $1/8\kappa_c$, is the inverse of Z_{2b}, when computed in Feynman gauge. Thus, in C_A, one may either define a new constant Z_A' by removing the factor of Z_{2b}, or else eliminate the u_0 which accompanies the leading factors of $\sqrt{2\kappa}$. We use the latter definition so that in the light-quark limit, where $e^{a\tilde{m}} \to 1$, the traditional normalization constant

is recovered. Since we evaluate Z_A using a boosted coupling, there is numerically little difference between the two approaches.

The lattice-continuum normalizations are then given explicitly by

$$C_A(\kappa_Q,\kappa_q)=Z_A\sqrt{2\kappa_Q e^{a\tilde{m}_Q}}\sqrt{2\kappa_q e^{a\tilde{m}_q}} \text{ (conventional)} , \tag{2.35}$$

$$\hat{C}_A(\kappa_q)=\hat{Z}_A C(a,m_Q)\sqrt{2\kappa_q e^{a\tilde{m}_q}} \text{ (static)} , \tag{2.36}$$

where $a\tilde{m}_{Q,q}$ are given by (2.33) with $\kappa=\kappa_{Q,q}$. With these definitions, the limiting expression (2.28) becomes

$$\phi_P \underset{\kappa_Q\to 0}{\sim} \hat{\phi}_P[1+O(\alpha_s)] . \tag{2.37}$$

Finally, let us consider this limit in detail in order to evaluate the extent of the mismatch at $O(\alpha_s)$. In C_A we can associate with each quark line a factor of

$$Z_2^{-1/2}\sqrt{2\kappa e^{a\tilde{m}}} ,$$

where $Z_2\equiv Z_{2a}Z_{2b}$. As a simplification, we use the perturbative relation $u_0=1/Z_{2b}$, despite the fact that in practice we evaluate u_0 nonperturbatively. We then find

$$Z_2^{-1/2}\sqrt{2\kappa_Q e^{a\tilde{m}_Q}}=Z_{2a}^{-1/2}\sqrt{u_0 2\kappa_Q}\left[\frac{1}{2u_0\kappa_Q}-3\right]^{1/2} \underset{\kappa_Q\to 0}{\sim} Z_{2a}^{-1/2} .$$

In the limit $\kappa_Q\to 0$, there is a full cancellation of tadpole corrections, leaving only the continuumlike wave function renormalization.

In the static-light renormalization $\hat{Z}_A$, the same "tadpole cancellation" already exists between the mass renormalization term discussed in Sec. II B and the wave function renormalization: i.e.,

$$\left[1-\frac{a\delta m^{(b)}}{2}\right]\hat{Z}_{2b}^{-1/2}=1$$

(the label "b" again denotes the tadpole contribution). This relation can be verified explicitly from the calculations in [12]. The remaining mismatch thus results purely from nontadpole perturbative corrections—both the wave function of the heavy (static) quark and the vertex graph for both theories. Although the nontadpole coefficients are small in the conventional calculation, they are not particularly so in the static one. At $\beta=6.3$ for example, using $a^{-1}\simeq 3$ GeV, $m_Q\simeq 5$ GeV and $g^2\simeq 1.6$, we find

$$\hat{C}_A/C_A(\kappa_Q\to 0)\simeq 1-\frac{g^2C_F}{16\pi^2}11.2 \simeq 0.85 .$$

Since we do not approach the limit $\kappa_Q\to 0$ in practice, we expect that the 15% difference seen here is an overestimate of the actual error incurred when interpolating between moderately heavy Wilson quarks (i.e., $am_Q\sim 1$) and the static limit. The systematic error from this effect is estimated concurrently with large-am errors in Sec. IV F.

E. Large-am errors at next-to-leading order

By interpolating between moderately heavy mesons and the static limit, we would like to compute the deviation from the scaling law (1.2) in the mass range of the D and B mesons. To do this, we adopt the phenomenological parametrization

$$\phi_P=c_0\left[1+\frac{c_1}{M_P}+\frac{c_2}{M_P^2}+O\left[\frac{1}{M_P^3}\right]\right] \tag{2.38}$$

and analyze the lattice results (both conventional heavy-light and static) in the form ϕ vs $1/M_P$. If the agreement between the two methods is good, we should find $c_0\approx\hat{\phi}$; c_1 will characterize the finite-mass correction. [We discuss the logarithmic correction to (2.38) in the following section.]

However, the removal of large-am lattice errors described in the previous section has only been made to leading order for a nonrelativistic Wilson quark (i.e., for the static component). It is possible to demonstrate explicitly, again by taking the infinite-mass limit, that the conventional calculation will not behave according to (2.38) because lattice effects distort the dynamics of the heavy quark. In the hopping parameter expansion, corrections to the leading behavior (2.25) are of order $2\kappa_Q$; thus, using (2.27), one finds that the limiting expression on the lattice will be

$$\phi_P \underset{\kappa_Q\to 0}{\sim} \hat{\phi}_P(1+Ce^{-aM_P}) .$$

At very large quark mass, the $1/M_P$ terms which should be present in the conventional amplitude will thus be exponentially suppressed by lattice artifacts.

In the nonrelativistic limit, the Wilson action can be rewritten by separating the quark and antiquark components through a Foldy-Wouthuysen transformation. After including the correct leading-order normalization for the field ψ, the action for quarks is expanded, in terms of a two-component spinor ϕ, in a discretized version of the form [20,19,18]

$$S_W=\phi^\dagger\left[m+D_0+\frac{1}{2m_2}\mathbf{D}^2+\frac{g}{4m_3}\sigma\cdot\mathbf{B}+\cdots\right]\phi . \tag{2.39}$$

In the limit that $am\ll 1$, the mass parameters in this expansion will all be approximately equal, and continuum physics will be well approximated at sufficiently weak couplings. However, (2.39) is obtained without placing any restriction on am, and when $am\gg 1$, ratios of the masses am, am_2, and am_3 diverge exponentially. We refer to this effect as the large-am error at next-to-leading order.

In the free theory, or in the mean-field approximation, the masses am_2 and am_3 can be easily calculated. The kinetic mass am_2 results from the dispersion relation

$$E(\mathbf{k})=m+\frac{\mathbf{k}^2}{2m_2}+\cdots ,$$

which is obtained from the calculation of the free Wilson quark propagator in the nonrelativistic limit. We find

$$am_2=\frac{e^{am}\sinh am}{\sinh am+1} . \tag{2.40}$$

The mean-field substitution $am\rightarrow a\tilde{m}$ in (2.40) defines $a\tilde{m}_2$, the tadpole-improved kinetic mass. The coefficient of the $\sigma\cdot\mathbf{B}$ term can be obtained by splitting $1/2m_2$, the coefficient of the $\mathbf{D}^2$ term, into two pieces, one which is contributed by the naive lattice action and one which is contributed by the Wilson term. The former is equivalent to $1/2m_3$, because the Wilson term adds no $\sigma\cdot\mathbf{B}$ piece to the action. The result is [19]

$$am_3=am_2(\sinh am+1) , \tag{2.41}$$

and tadpole corrections are again included via the mean-field method to define $a\tilde{m}_3$.

The nonrelativistic limit of the Wilson action (2.39) is similar in form to the nonrelativistic QCD (NRQCD) action proposed recently by Lepage and Thacker for the study of heavy-quark bound states [22]. In NRQCD, the action is discretized *a priori* in this form; the coefficients of the higher-dimensional operators are free to be tuned in order to match the effective theory to full QCD. Although the standard Wilson action does not afford this freedom, it is, under certain conditions, suitable for the simulation of nonrelativistic quarks even when $am\gg 1$ [20]. For example, in the case of quarkonium (i.e., a heavy-heavy meson), the $\sigma\cdot\mathbf{B}$ interactions are suppressed by a factor of the velocity squared and thus can be neglected in the lowest-order calculation. This fact follows from the nonrelativistic nature of the bound state. Furthermore, the rest mass m only contributes an overall constant to the action; it is irrelevant in the calculation of transition amplitudes. (In NRQCD, m is typically removed from the theory from the beginning.) Thus, if one computes an arbitrary heavy-heavy amplitude as a function of the meson pole mass, say $A(M)$, then to lowest order, M sees the rest mass $\tilde{m}$, whereas A sees the kinetic mass $\tilde{m}_2$. This error can be approximately corrected by adjusting the meson mass:

$$aM\rightarrow aM'=aM+(a\tilde{m}_2-a\tilde{m}) . \tag{2.42}$$

Then $A(M')$ gives the correct functional dependence, within additional $O(\alpha_s)$ corrections which are not included by the tadpole approximation.

In the current heavy-light analysis, we make the shift (2.42) in the pole mass M_P and fit to the functional form Eq. (2.38). This is our best attempt to remove large-am errors at next-to-leading order. However, because the light quark is relativistic, the $\sigma\cdot\mathbf{B}$ term is no longer suppressed relative to the kinetic one. Since $a\tilde{m}_3\neq a\tilde{m}_2$, the mass shift is insufficient to completely correct for the large-am error in the same sense as described above; there will be some additional systematic error in the fitted coefficient c_1. The error induced by this effect in the calculation of f_B and f_D will depend on a number of factors—e.g., the overall size of the deviations from the asymptotic limit (1.2) and the extent to which $a\tilde{m}_3$ differs from $a\tilde{m}_2$ in the mass region where the conventional method is used. We estimate this error from the numerical results in Sec. IV F.

F. Logarithmic corrections

Finite logarithms in the matrix element of the full-QCD axial current become the source of an additional ultraviolet divergence in the static limit [2]. This fact results in an explicit logarithmic dependence on the heavy quark mass in the static-light axial renormalization constant, which we have written as the factor $C(a,m)$ given by Eq. (2.12). If sufficiently fine lattices could be constructed, so that $am_Q\ll 1$ even as the scaling region (1.2) were approached, then the logarithmic corrections would be entirely contained in the lattice matrix element of the conventional calculation. In the opposite extreme, where $\kappa_Q\rightarrow 0$ and $am_Q\gg 1$, the logarithmic dependence is lost entirely, as part of the "nontadpole" $O(\alpha_s)$ corrections which have not been included.

Anticipating improved computations, where the former of these two limits may be approached, we analyze the numerical data assuming the presence of the full leading logarithmic correction. To do this, we eliminate the factor $C(a,m_Q)$ from the renormalization constant of the static-light axial current given by Eq. (2.36) ($\hat{\phi}$ is thus well defined at $1/M_P=0$) and divide it, in the form $C(a,M_P)$, from the conventional amplitude. In this form, ϕ is fit to a quadratic in $1/M_P$, as implied by Eq. (2.38). To compute a physical result, e.g., ϕ_B, we interpolate the fit to the appropriate mass and then multiply by the logarithmic correction, e.g., $C(a,M_B)$. Insofar as the logarithmic dependence on the quark mass may be absent from the lattice results in the region where am_Q is large, this procedure too will involve some systematic error. This error is akin to the mismatch in the constant terms of the leading perturbative correction discussed at the end of Sec. II D but is considerably smaller. At $\beta=6.3$, for example, $C(a,M_B)$ itself is a correction of only a few percent. The procedure described in Sec. IV F is an estimate of the cumulative effect of all such systematic effects which alter ϕ_P in the region of large am_Q.

III. NUMERICAL TECHNIQUES

A. Smeared sources

The basic techniques and advantages of using nonlocal, or "smeared" sources in a fixed gauge have been well established in the recent literature [23]. In this section we discuss briefly our use of Coulomb-gauge, "wall-source" (WS) propagators [24], which we use to compute our best results from the conventional method at $\beta=6.3$. We also use, for the static limit, a method of smearing which utilizes standard point-source propagators, which we will refer to as "cube" smearing for reasons which will become obvious in the following section. For the conventional method, at all couplings other than $\beta=6.3$, we use a standard point-source construction of the correlators,

which was given explicitly in Sec. II A.

The wall-source propagator $\tilde{S}$ is defined by

$$\tilde{S}(\mathbf{x},t;t_0;U)=\frac{1}{V}\sum_{\mathbf{y}}\langle\psi(\mathbf{x},t)\bar{\psi}(\mathbf{y},t_0)\rangle_U\ , \tag{3.1}$$

and is computed from the Wilson action $\mathcal{S}_W=\bar{\psi}S^{-1}\psi$ through the solution of the equation

$$\sum_z S^{-1}(x;z;U)\tilde{S}(z;t_0;U)=\frac{1}{V}\delta_{t,t_0}\sum_{\mathbf{y}}(\delta^3_{\mathbf{x},\mathbf{y}})\ , \tag{3.2}$$

where V represents the spatial volume of the lattice, and we have suppressed color and spin indices. The technique is trivially implemented by the replacement of the usual single-site δ function with the sum of δ functions in the matrix inversion program.

One must then construct a smeared interpolating operator χ so that the correlation functions analogous to those defined by (2.2) reduce to contractions involving only wall-source propagators. Since the gauge-dependent overlap function $\langle 0|\chi^\dagger|P\rangle$ is removed from the final physical amplitude, the extraction of the decay constant and the normalization issues discussed in the previous section remain unaffected. For reasons which we explain shortly, we construct a pair of operators, denoted by the two signs in the definition

$$\chi^\dagger_{W_\pm}(t)=\frac{1}{V^2}\sum_{\mathbf{x},\mathbf{y}}\bar{Q}(\mathbf{x},t)\left[\frac{1\pm\gamma_0}{2}\right]\gamma_5 q(\mathbf{y},t)\ . \tag{3.3}$$

They are used as follows. We compute WS propagators from a "left" source t_{0L} (i.e., near the edge defined as $t=0$) for the upper two source spin components only. Similarly, we compute propagators from a "right" source t_{0R} (near the opposite edge) for the lower two source spins. Note that we have used Dirichlet, not periodic, boundary conditions in the time direction. We then obtain the wall-source correlators by replacing χ, as defined by (2.3b), with the smeared version (3.3) in Eqs. (2.2). Thus we compute

$$G_A^{W_\pm}(t,t_0)=\left\langle\sum_{\mathbf{x}}\mathrm{Tr}[\tilde{S}_q^{(\pm)\dagger}(\mathbf{x},t;t_0;U)\times\gamma_0\tilde{S}_Q^{(\pm)}(\mathbf{x},t;t_0;U)]\right\rangle_{\{U\}} \tag{3.4a}$$

and

$$G_B^{W_\pm}(t,t_0)=\frac{1}{V}\left\langle\mathrm{Tr}\left[\sum_{\mathbf{x}}\tilde{S}_q^{(\pm\pm)\dagger}(\mathbf{x},t;t_0;U)\times\sum_{\mathbf{y}}\tilde{S}_Q^{(\pm\pm)}(\mathbf{y},t;t_0;U)\right]\right\rangle_{\{U\}} \tag{3.4b}$$

where we used the abbreviated notation

$$S^{(\pm)}\equiv S\left[\frac{1\pm\gamma_0}{2}\right]$$

and

$$S^{(\pm\pm)}\equiv\left[\frac{1\pm\gamma_0}{2}\right]S\left[\frac{1\pm\gamma_0}{2}\right]\ . \tag{3.5}$$

Note that $G_B^{W_\pm}(t,t_0)$ has just two spins at both source and sink—as usual, $G_B^{W_\pm}(t,t_0)$ must be "diagonal" (same source and sink) so that the overlap of the interpolating field with the lowest state can be determined. For $t_0=t_{0L}$ we use the source χ_+ so that both of the correlation functions need only the upper two source spins of the propagators; they are analyzed for forward propagation $t>t_0$. Similarly, for $t_0=t_{0R}$ we use the source χ_-. These correlators need only the lower two spins and are analyzed for backward propagation $t<t_0$. So the amount of computing required in terms of propagator generation is the same as for the standard single-source approach: we have doubled the number of source times and halved the number of spins.

This scheme has been chosen in anticipation of the B parameter calculation, where the matrix element is computed from a lattice "figure-eight" graph containing a local four-fermion operator at its intersection point and meson interpolating operators at either edge. We have altered our usual convention for propagator generation, i.e., placing the source at the center of the lattice, because in this case the local operator of interest must be constructed using the *sink* point of the wall-source propagators. They must therefore originate from either side of the lattice center. For the decay constant calculation, however, this scheme has provided two sets of propagators for each configuration, $\tilde{S}^{(+)}(\mathbf{x},t;t_{0L};U)$ and $\tilde{S}^{(-)}(\mathbf{x},t;t_{0R};U)$.

Since our wall sources at t_{0L} and t_{0R} are widely separated, we expect that the forward-backward pairs for a given configuration will not be strongly correlated. In using covariant fits as we have done, it is advantageous to be able to treat these correlators as independent, since the total number of time slices that can be included in the fit is limited by the number of independent correlators. To test for independence on our 20 configurations at $\beta=6.3$, we have compared, for four different quantities at $\kappa=0.150$, the results of covariant fits performed two ways: (1) treating forward and backward correlators as independent, and (2) using time reversal symmetry as in Ref. [3] to average the forward-backward pairs on each configuration before fitting. The results for the pion mass, pion decay constant, static-light mass, and static-light decay constant, each computed using several different fitting intervals, are consistent within our statistics with the independence of the forward and backward pairs. In particular, the central values of the two methods agree within errors; the difference between the errors varies by typically 10–30%; and the sign of the difference varies in an apparently random way. This is consistent with what one would expect for 40 uncorrelated data points.

B. Smearing techniques for static quarks

It has been observed in previous static computations that point-source correlation functions, such as that defined by (2.14), fail to show ground-state dominance at sufficiently early times and at large times are saturated with noise. This problem has prompted the use of smeared sources which, it is hoped, may be tuned to have the best possible overlap with the ground state, so that it dominates sufficiently in the early time slices. Qualitatively, at least, this program has been successful [25,7–10,26]. Nevertheless, it is interesting to note the source of the problem in terms of a simple analysis of the Euclidean correlators.

Lepage has outlined a method for estimating signal-to-noise in discussing the proton on the lattice [27]. First, consider $G_\pi(t)$, a single-configuration contraction of two light-quark propagators. The computed estimate of the "pion" correlation function is defined by the average over N configurations, which at large times falls exponentially: $\langle G_\pi(t)\rangle \sim Ze^{-aM_\pi t}$. The expectation for the noise is given by the formula $\sigma_G^2=(1/N)(\langle G_\pi^2\rangle-\langle G_\pi\rangle^2)$. Since both $\langle G_\pi^2\rangle$ and $\langle G_\pi\rangle^2$ overlap with a two-pion state, the signal-to-noise ratio (SNR) is a constant at large times:

$$\lim_{t\to\infty}\frac{\langle G\rangle}{\sigma_G}\sim\sqrt{N}\quad\text{(pion)}\,.$$

In contrast, consider a similar analysis of the static-light correlator [28,20,29]. In this case, the signal falls exponentially with the (divergent) mass parameter $a\mathcal{E}_0$: $\langle G\rangle\sim Ze^{-a\mathcal{E}_0 t}$. The noise, however, is dominated in the large-time region by $\langle G^2\rangle$, which has a nonzero overlap with a single pion, as depicted in Fig. 1. The static lines effectively cancel, and $\sigma_G^2\sim e^{-aM_\pi t}$. The SNR is thus given by

$$\lim_{t\to\infty}\frac{\langle G\rangle}{\sigma_G}\sim\sqrt{N}\exp\left[-a\left[\mathcal{E}_0-\frac{M_\pi}{2}\right]t\right]$$

$$\text{(static-light)}\,. \qquad (3.6)$$

Typically, the binding energy $a\mathcal{E}_0$ is much larger than half the pion mass. For example, at $\beta=6.0$ with $\kappa_q=0.155$, we find $a\mathcal{E}_0\simeq 0.6$, whereas the corresponding pion mass is $aM_\pi\simeq 0.3$. An essential point to note is that the use of smeared sources may optimize the ground-state signal in the earlier time slices, but it will not change the behavior described by Eq. (3.6).

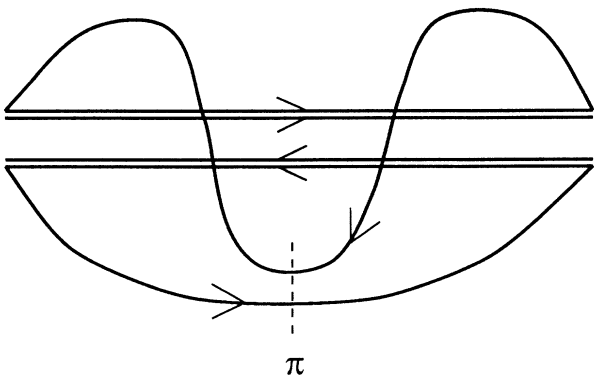

FIG. 1. "Noise correlator" for the static-light channel.

We have used two types of sources for the static computations. The first is a wall source (used only at $\beta=6.3$) and is a straightforward adaptation of the technique outlined in the previous section. The heavy Wilson quark field $Q(x)$ in the interpolating operator (3.3) is replaced with the static field $h(x)$ (or, for backward movers, the analogous antiquark field); the sums necessary to construct the correlation functions $\hat{G}_A^{W_\pm}$ and $\hat{G}_B^{W_\pm}$ are easily computed due to the trivial nature of the static-quark propagator.

The second type of smeared operator is introduced in order to accommodate point-source, rather than wall-source, light-quark propagators. We refer to it as a "cube" and define it by

$$\hat{\chi}_{n+}^\dagger(\mathbf{x},t)=\frac{1}{n^3}\sum_{\mathbf{z}}^{[V_n]}\bar{h}(\mathbf{x}+\mathbf{z},t)\gamma_5 q(\mathbf{x},t)\,, \qquad (3.7)$$

where $[V_n]$ denotes the sites of the cube centered around $\mathbf{x}$. We have written only the static *quark* form of the operator; the antiquark construction is analogous. As before, we compute the forward-moving correlators from χ_{n+} and the backward-moving correlators from χ_{n-}. They are given by

$$\hat{G}_A^{S_\pm}(t,t_0)=\frac{1}{n^3}\left\langle\sum_{\mathbf{z}}\mathrm{Tr}[S_q^{(\pm)\dagger}(\mathbf{z},t;\mathbf{0},t_0;U)\times\mathcal{P}^\pm(\mathbf{z},t,t_0;U)]\right\rangle_{\{U\}} \qquad (3.8a)$$

and

$$\hat{G}_B^{S_\pm}(t,t_0)=\frac{1}{n^6}\left\langle\sum_{\mathbf{z},\mathbf{z}'}\mathrm{Tr}[S_q^{(\pm)\dagger}(\mathbf{z}+\mathbf{z}',t;\mathbf{0},t_0;U)\times\mathcal{P}^\pm(\mathbf{z}',t,t_0;U)]\right\rangle_{\{U\}}\,, \qquad (3.8b)$$

where we have included the Dirac structure $(1+\gamma_0)/2$ $[(1-\gamma_0)/2]$ of the static quark (antiquark) propagator through the notation (3.5) applied to the light-quark propagator.

C. Fitting and jackknife analysis

We compute statistical errors using the jackknife technique. Our discussion here will be limited to a brief description of (1) the inclusion of correlations in the numerical data, i.e., the use of "covariant" fits, and (2) the specific parametrization (i.e., fitting function) for the correlation functions. To facilitate this, let us define any jackknifed quantity Q with the notation $Q\equiv\{\bar{Q},Q_i\}$, where $\bar{Q}$ results from an analysis of the full average of N configurations, and Q_i from an analysis of the ith "subset average" of configurations, where one or more has been removed.

The (estimated) covariance matrix used in the χ^2

minimization fitting routine is then defined through a straightforward generalization of the standard formula [30]. For an m-elimination jackknifed quantity $Q(k)$, where k denotes some external parameter dependence, we write it as

$$C_Q(k_1,k_2)=\left[\frac{N}{m}-1\right] \times\langle[Q_i(k_1)-\bar{Q}(k_1)][Q_i(k_2)-\bar{Q}(k_2)]\rangle \ . \tag{3.9}$$

By definition, correlation functions are computed by averaging over individual configurations. In this case, and for $m=1$, Eq. (3.9) reduces identically to the standard covariance formula of Ref. [30]. This, of course, is not the case for a quantity which is computed *from* an average, such as a fitted mass.

In fitting a quantity $Q(k)$ to some theoretically expected functional form, $F(k, \mathbf{A})$ ($\mathbf{A}$ is the set of parameters to be fit), the fit is jackknifed, but the fits to $\bar{Q}$ and the Q_i use the same inverse covariance matrix C_Q^{-1}. Each level of fits [e.g., correlation functions, $f(\kappa_q)$ vs $1/\kappa_q$, etc.] takes into account correlations in the numerical data and produces a meaningful $\chi^2/N_{\rm DF}$ (χ^2 per degree of freedom). This method thus gives an indication of how different systematic errors affect the calculation at each stage, and, as a practical matter, clearly requires many fewer configurations than would the inclusion of all correlations simultaneously.

Our fits to the correlators G_A and G_B are "coupled," i.e., made simultaneously and with identical mass parameters. Thus at the stage of a single lattice meson we compute all correlations, including those between the two channels G_A and G_B. To denote this, we assign a dummy index a to the time coordinate. It takes on the values $a=(A,B)$—i.e., we define $G(t^A)\equiv G_A(t^A)$ and $G(t^B)\equiv G_B(t^B)$. The meaning of the covariance matrix $C_G(t_1^a,t_2^b)$ is then immediately apparent. Depending on the type of correlator, we compute one of two types of fits (the choice is specified in Sec. IV). We denote them loosely as the "single-state" fit

$$\chi^2_{\rm min}[G(t^a)-\zeta_a e^{-aMt^a}]\rightarrow M,\zeta_A,\zeta_B \tag{3.10}$$

and the "two-state" fit

$$\chi^2_{\rm min}[G(t^a)-(\zeta_a e^{-aMt^a}+\zeta'_a e^{-aM't^a})] \rightarrow M,M',\zeta_A,\zeta'_A,\zeta_B,\zeta'_B \ , \tag{3.11}$$

where the quantities on the right denote jackknife fit parameters.

We invert the covariance matrix using the lower-upper (LU) algorithm and improve the solution, to correct for accumulated roundoff error, using the iterated improvement algorithm of Ref. [31]. Roundoff errors are further reduced by always fitting to the log of the data—this avoids a covariance matrix whose elements span several orders of magnitude. As the total number of time slices included in a single fit nears the numbers of configurations, the estimated covariance matrix will become singular. However, we use covariant fits only where our statistical sample is large enough to avoid this problem. [Recall that the number of configurations is effectively doubled by treating forward and backward movers independently. In the most extreme case, the two-state fit at $\beta=6.3$, we typically used $(N_{t_A}+N_{t_B})\simeq 25-33$, whereas $2N_{\rm config}=40$.] We did not find it necessary or even advantageous to further increase the number of time slices included in the fits, and this inversion method was generally satisfactory.

Nevertheless, it appears to us that there remain errors associated with the computed estimate of the covariance matrix, Eq. (3.9), which are not necessarily reflected by the jackknife, although we do not have a large enough statistical sample to verify this assertion. In this regard, our findings are qualitatively similar to those of other groups which have made more systematic studies on covariant fitting techniques (see, for example, Ref. [32]). We attempt to include such variations as part of the systematic error estimate described below.

D. Fitting errors

We categorize fitting errors as those arising from the following sources: (1) "finite-time" contamination of the correlation functions from higher states or the boundary, (2) the computation of the covariance matrix, and (3) extrapolations to the chiral or strange limits. To estimate a combined fitting error for a given result, we compile a sample of alternate ones, each computed from a modified analysis. This set of results is subject to a cut of $\chi^2/N_{\rm DF}\leq 2$, pertaining to the last relevant fit which produced it. We then compute the standard deviation of the alternates from what we have chosen as the central value. The alternate analyses are modified in one or more of the following ways.

Extrapolations. The central value of a quantity which is obtained from an extrapolation to the physical pion or kaon is computed using a fit to the data from the three lightest quark masses. Alternates are computed by fitting to the lightest two masses, and at $\beta=6.0$ the heavier two were also used.

Type of fits. For the wall-source, heavy-light correlators at $\beta=6.3$, we use the two-state fit for central values (Secs. IV C and IV D). In this case alternates are computed from single-state fits over later time intervals to sample finite-time effects.

Covariance matrix. Central values are computed using the single-elimination jackknife. Two- and sometimes four-elimination jackknifes are sampled in order to vary the computation of the covariance matrix. In addition, we compare the time-reversed "folded" and "unfolded" analyses in cases where the number of time slices vs configurations permits.

Fit intervals. Time slice intervals for central value fits were chosen based on an examination of the plateau in the effective mass and, in the case of covariant fits, the $\chi^2/N_{\rm DF}$. Alternates are computed by changing the size and location of these intervals. Naively, the variation in results that this produces is indicative of finite-time systematics; however, we believe it again to be a reflection of

the error in the covariance matrix. When noncovariant fits are used, the shifts typically have a negligible effect in comparison to the jackknife error.

IV. ANALYSIS AND RESULTS

We now discuss the details of the computations, present qualitative and quantitative results, and estimate bounds for various systematic errors. We begin by providing the essential parameters pertaining to the gauge configuration and propagator generation, and then present the analysis in various stages: light mesons (i.e., the pion and kaon), conventional heavy-light states, static-light, the combined analysis for $1/M_P$ corrections to the asymptotic scaling law (1.2) and the calculation of physical amplitudes, and finally bounds for large-am and scale errors. In practice, the calculation was split up in this fashion, but in such a way so that results passed from one stage to the next (e.g., a^{-1}, κ_c, etc.) could be included in the jackknifed analysis for statistical errors.

In the sections pertaining to the fits to the correlation functions, we refer extensively to the effective mass as a way of determining the point of ground-state saturation. For a correlator $G(t)$, the basic definition of the effective mass is

$$aM(t)=\ln\left[\frac{G(t)}{G(t+1)}\right]. \tag{4.1}$$

Where a single state dominates $G(t)$, $aM(t)$ has a plateau. [We actually use single-exponential, uncorrelated fits over three time slices, i.e., centered at t, to which we associate the fitted mass parameter $M(t)$. In practice, there is very little difference between the results of this method and the discrete logarithmic derivative given above.]

A. Simulation parameters

1. $\beta=6.3$

We have generated twenty 24^4 Coulomb-gauge lattices at $\beta=6.3$, one set of five with the pseudo-heat-bath algorithm (6 K passes to thermalize, 2 K passes separation), and three sets of five with a combination "3–6 overrelaxed + 1 pseudo-heat-bath" algorithm (4 K total passes to thermalize, 2–2.2 K total passes separation). Two sets had hot starts, and two had cold starts. From these lattices we have generated both wall-source and point-source propagators after extending the gauge configurations in the time direction using the periodicity. In all propagator generation, we have employed spatially periodic and fixed time boundary conditions. In three of the sets, relative temporal shifts were introduced to further randomize the sample. Wall-source propagators were made at $24^3\times55$ for two source locations, $\tilde{S}^{(+)}$ from $t_{0L}=13$ and $\tilde{S}^{(-)}$ from $t_{0R}=41$ [sites labeled $t=(0,54)$ and using the notation of Sec. III]. Point-source propagators were made at $24^3\times61$ with a central source ($t_0=30$). In both cases, the time boundary condition was Dirichlet.

In order to measure the overlap functions of the wall-source correlators, the source must be placed sufficiently far from the lattice edge in order to avoid any distortion from the boundary. Checks to determine a sufficient displacement were made as follows. Two propagators, sizes $24^3\times55$ and $24^3\times45$, were computed at $\kappa=0.150$ from the same configuration, with the wall source in each case at the same trial position t_{0L} as measured from the "left" edge of the lattice. From these propagators, degenerate correlators $G_B^{W_\pm}$ were computed; call them G_{55} and G_{45}. From each we computed the local masses $M(t)$, using (4.1), and the local amplitude, $\zeta(t)=G(t)\exp[tM(t)]$, where t labels the distance from the source. The corresponding residues $\zeta_{55}(t)$ and $\zeta_{45}(t)$ were compared as t was increased until the point $t=\tilde{t}$ where the difference exceeded 1%. The number of slices between and including that labeled by $\tilde{t}$ and the "right" edge of the shorter lattice was taken as the necessary source displacement T. We found $T=13$ and thus used $t_{0L}=13$ and $t_{0R}=41$ for the $24^3\times55$ propagators. Since mass fluctuations are amplified exponentially in the correlator residues, this test is far more stringent than the analogous comparison of the local masses themselves.

2. $\beta=6.0$

At $\beta=6.0$ we have constructed and analyzed two independent data sets. The first consists of nineteen configurations of gauge size $16^3\times40$. Eight of the nineteen were generated using the pseudo-heat-bath (PHB) algorithm, 2 K to thermalize, 1 K separation. The remaining eleven configurations were generated using an overrelaxed-metropolis (OM) algorithm with a 600-sweep separation. Point-source propagators for light-quark masses only were generated at $16^3\times39$ with a central source.

The second set consists of eight configurations of gauge size $24^3\times40$. These have 2 K OM sweeps for thermalization and 1 K sweeps for subsequent separations. Point-source propagators were generated for heavy and light quark masses at $24^3\times39$ with a central source.

3. $\beta=5.7$

At $\beta=5.7$ a single analysis was made on the combined data set of 32 configurations described in the following table:

Configurations	Gauge	Quark
16 PHB	$16^3\times24$	$16^3\times25$
4 PHB	$16^3\times24$	$16^3\times33$
12 PHB	$16^3\times32$	$16^3\times33$

Propagators were generated with a central point source for light quark masses only. The analysis is limited by the smaller time dimension, so we refer to them as $16^3\times25$. In each case the configurations were separated by 1 K passes.

B. Light mesons

An analysis of the light pseudoscalars was done on each of the data sets listed above in order to compute

f_K/f_π and to obtain the (jackknifed) parameters needed for the heavy-light computations. In this section, we discuss several aspects of this analysis. First, we focus on the quality of the data at $\beta=6.3$, discuss some details of the fits to the correlation functions, and compare wall sources with point sources. (We have used wall sources only at $\beta=6.3$.) Second, we discuss the extrapolation of the raw numbers obtained from the correlator fits to physical values of the quark mass. Lastly, we present results for f_K/f_π and estimate its scaling error at $\beta=6.3$. The numerical results are provided in Tables I–V. In each case we provide the breakdown $af=C_A\times af^{(0)}$, where C_A includes factors of $\sqrt{2\kappa}$ and is given explicitly by Eq. (2.35), so that the bare lattice results and their errors can be obtained trivially.

The covariant single state fit (3.10) was used to compute the ground state masses and decay amplitudes in the chiral regime. Statistical errors were obtained from the single elimination jackknife, treating the forward- and backward-moving correlators as separate configurations. We show the effective masses and best fit for the $\kappa=0.150$, wall-source pion at $\beta=6.3$ in Fig. 2. The mass of the wall-point correlator (G_A^W) appears to be asymptotic after a displacement of approximately $t=12$; however, it contains fluctuations which make an assessment of systematic finite-time effects difficult. We found that the most satisfactory fits in terms of minimum $\chi^2/N_{\rm DF}$ were obtained from intervals displaced further from the source; for final results we chose $t_{\rm min}=15$. Note also that the wall-wall correlator (G_B^W) is much noisier than the wall point. This is due to the extra summation in Eq. (3.4b). It produces a relative increase in the number of contractions between quark propagators whose spatial separation at the source and sink is much larger than the size of the state, and the correlation function is thus subject to large unphysical fluctuations in the gauge links on a given time slice. This feature has previously been found to be true also of Wuppertal sources [32].

Because of the differences in the construction of our wall- and point-source propagators it is difficult to make a clear comparison between the two methods. Qualitatively, as seen in Fig. 3, the point-source effective masses approach ground-state saturation more slowly. However, because the central placement of the point source results in a smaller temporal length, we have used a similar fit interval as for the wall-source analysis in order to remain sufficiently far from the boundary. Clearly, however, the plateaus in the point-source case are not very convincing, and a large systematic error would result if we were forced to rely on these data alone. Results extracted using $t=(15,21)$ are given in Table II and may be compared to the wall-source results [from fits over $t=(15,24)$] in Table I. The two methods produce consistent results within errors. Because of the better quality of the effective-mass plateaus, we use the wall sources for our final results. In addition, the errors in af_π from the wall-source analysis are smaller, which results in a better scale determination.

The analysis of the light mesons proceeds according to a standard extrapolation scheme, motivated by the leading order predictions of chiral perturbation theory. Define the lattice quark mass as $am_0(\kappa)=1/2\kappa-1/2\kappa_c$, and denote the fitted masses and decay constants of the degenerate mesons as $aM(\kappa)$ and $af(\kappa)$. We fit $(aM)^2$ linearly in the quark mass, i.e., linearly in $1/\kappa$, and extrapolate the fit to $aM=0$ where we extract the critical hopping parameter κ_c. Similarly, we fit af linearly in $1/\kappa$ and extrapolate to $1/\kappa=1/\kappa_c$ to compute af_π. The scale is determined from $a_{f_\pi}^{-1}=132$ MeV$/(af_\pi)$. The above procedure can be iterated, extrapolating instead to the physical pion mass in order to determine κ_c. Although we in fact do this, the resulting shift in κ_c and a^{-1} is in all cases smaller than the statistical error.

TABLE I. Light meson results at $\beta=6.3$ (wall source). Fits were covariant, single-state, over $t=(15,24)$ for both correlators. The statistical error is from the jackknife of the fit; the systematic (fitting) error is estimated as described in Sec. III D.

κ	$\chi^2/N_{\rm DF}$	aM	C_A	$af^{(0)}$	$af\times 10$
0.149	2.0	0.316(2)±0.003	0.250	0.263	0.658(16)±0.017
0.150	2.8	0.247(3)±0.003	0.245	0.234	0.573(15)±0.014
0.1507	2.8	0.188(4)±0.004	0.242	0.203	0.491(13)±0.013
κ_c		$a\times m_\pi$[a]			0.411(12)±0.022[b]

κ_1	κ_2	$\chi^2/N_{\rm DF}$	aM	C_A	$af^{(0)}$	$af\times 10$
0.149	0.150	2.4	0.283(2)±0.003	0.247	0.249	0.615(15)±0.018
	0.1507	2.9	0.258(3)±0.003	0.246	0.234	0.574(15)±0.015
	κ_c		0.222(2)±0.005			0.535(14)±0.024
0.150	0.1507	3.1	0.218(3)±0.004	0.243	0.218	0.531(14)±0.011
	κ_c		0.176(2)±0.003			0.491(13)±0.017
0.1507	κ_c		0.139(2)±0.004			0.450(12)±0.018
κ_s	κ_c		$a\times m_K$[c]			0.466(15)±0.021[d]

[a] $\kappa_c=0.15158(5)\pm.00007$.
[b] $a^{-1}=3.21(9)\pm0.17$ GeV.
[c] $\kappa_s=0.15043(7)\pm0.00013$.
[d] $f_K/f_\pi=1.134(6)\pm0.015$.

TABLE II. Light meson results at $\beta=6.3$ (point source). Fits were covariant, single-state, over $t=(15,21)$ for both correlators.

κ	$\chi^2/N_{\rm DF}$	aM	C_A	$af^{(0)}$	$af\times 10$
0.149	1.9	0.316(2)±0.002	0.250	0.279	0.696(25)±0.022
0.150	1.6	0.247(2)±0.002	0.245	0.243	0.596(28)±0.026
0.1507	1.6	0.192(2)±0.002	0.242	0.219	0.529(31)±0.019
κ_c		$a\times m_\pi$ [a]			0.438(38)±0.025[b]

κ_1	κ_2	χ^2	aM	C_A	$af^{(0)}$	$af\times 10$
0.149	0.150	1.8	0.283(2)±0.002	0.248	0.263	0.651(26)±0.019
	0.1507	1.6	0.258(2)±0.002	0.246	0.245	0.604(28)±0.022
	κ_c		0.220(2)±0.003			0.559(31)±0.024
0.150	0.1507	1.4	0.221(2)±0.002	0.244	0.228	0.556(30)±0.022
	κ_c		0.178(1)±0.002			0.505(33)±0.018
0.1507	κ_c		0.143(2)±0.003			0.487(35)±0.024
κ_s	κ_c		$a\times m_K$ [c]			0.500(45)±0.028[d]

[a] $\kappa_c=0.15163(3)\pm0.00004$.
[b] $a^{-1}=3.01(26)\pm0.18$ GeV.
[c] $\kappa_s=0.15029(28)\pm0.00016$.
[d] $f_K/f_\pi=1.142(13)\pm0.034$.

An additional level of fits and extrapolations is required in order to determine κ_s, the strange quark hopping parameter, and to compute f_K. For each combination of light quarks (κ_1,κ_2) we compute $(aM)^2_{\kappa_1,\kappa_2}$ and af_{κ_1,κ_2}. We fit both quantities linearly in $1/\kappa_2$ and extrapolate to $1/\kappa_2=1/\kappa_c$. We then fit $(aM)^2_{\kappa_1,\kappa_c}$ linearly in $1/\kappa_1$ and interpolate to the physical kaon mass in order to determine κ_s. Finally, we compute af_K by fitting af_{κ_1,κ_c} linearly in $1/\kappa_1$ and interpolating to $1/\kappa_1=1/\kappa_s$. The four quantities aM_π, aM_K, af_π, and af_K are thus used to determine three parameters κ_c, κ_s, and a^{-1} and make one prediction, f_K.

Our fitting technique (Sec. III C) would in principle allow us to include the inter-κ correlations and thus quote a meaningful $\chi^2/N_{\rm DF}$ in the chiral fits described above. In fact we have not done so, because we find that the correlated fits of $(aM)^2$ and af in many cases do not converge to a sensible result and often give a large $\chi^2/N_{\rm DF}$. The most likely cause of this is that the jackknife procedure underestimates the errors since it does not include systematic effects (e.g., finite volume and finite time errors) which may affect the results at different quark masses in a nonuniform way. Assuming this to be the case, we turn off the correlations to obtain the best approximation to the leading chiral behavior which the linear fit functions

TABLE III. Light meson results at $\beta=6.0$, $24^3\times 39$ (point source). Fits were noncovariant, single-state, over $t=(9,14)$ for both correlators.

κ	aM	C_A	$af^{(0)}$	$af\times 10$
0.152	0.489(9)±0.001	0.263	0.424	1.11(6)±0.01
0.154	0.374(10)±0.001	0.254	0.354	0.90(5)±0.00
0.155	0.311(9)±0.002	0.249	0.315	0.79(6)±0.01
κ_c	$a\times m_\pi$ [a]			0.58(9)±0.02[b]

κ_1	κ_2	aM	C_A	$af^{(0)}$	$af\times 10$
0.152	0.154	0.434(9)±0.001	0.258	0.388	1.00(5)±0.01
	0.155	0.405(10)±0.000	0.256	0.366	0.94(5)±0.00
	κ_c	0.339(8)±0.004			0.82(6)±0.02
0.154	0.155	0.343(9)±0.001	0.251	0.334	0.84(6)±0.01
	κ_c	0.268(7)±0.003			0.74(7)±0.01
0.155	κ_c	0.230(5)±0.002			0.69(8)±0.01
κ_s	κ_c	$a\times m_K$ [c]			0.68(11)±0.02[d]

[a] $\kappa_c=0.1570(1)\pm0.0002$.
[b] $a^{-1}=2.3(4)\pm0.1$ GeV.
[c] $\kappa_s=0.1553(8)\pm0.0002$.
[d] $f_K/f_\pi=1.18(2)\pm0.01$.

TABLE IV. Light meson results at $\beta=6.0$, $16^3\times 39$ (point source). Fits were covariant, single-state, over $t=(9,14)$ for both correlators.

κ	$\chi^2/N_{\rm DF}$	aM	C_A	$af^{(0)}$	$af\times 10$
0.152	1.0	0.497(3)±0.002	0.263	0.406	1.07(4)±0.02
0.154	1.2	0.380(3)±0.005	0.254	0.384	0.97(5)±0.03
0.155	1.2	0.311(3)±0.010	0.249	0.343	0.86(6)±0.03
κ_c		$a\times m_\pi$[a]			0.63(8)±0.11[b]

κ_1	κ_2	$\chi^2/N_{\rm DF}$	aM	C_A	$af^{(0)}$	$af\times 10$
0.152	0.154	0.9	0.443(3)±0.002	0.258	0.389	1.00(5)±0.02
	0.155	1.1	0.412(3)±0.004	0.256	0.382	0.98(5)±0.03
	κ_c		0.346(5)±0.006			0.92(6)±0.05
0.154	0.155	1.2	0.346(3)±0.008	0.251	0.368	0.92(5)±0.03
	κ_c		0.270(3)±0.007			0.83(7)±0.05
0.155	κ_c		0.227(2)±0.005			0.72(7)±0.05
κ_s	κ_c		$a\times m_K$[c]			0.75(11)±0.10[d]

[a] $\kappa_c=0.1570(1)\pm 0.0002$.
[b] $a^{-1}=2.1(3)\pm 0.3$ GeV.
[c] $\kappa_s=0.1548(7)\pm 0.0008$.
[d] $f_K/f_\pi=1.20(3)\pm 0.05$.

are intended to model. Typical chiral extrapolations (for the heavy-light case) are shown in Figs. 4 and 5. Note that the fits to straight lines look excellent to the eye; yet correlated fits (when they converge at all) would still give a large $\chi^2/N_{\rm DF}$. For example, for the degenerate light-light case, correlated fits at $\beta=6.3$ give $\chi^2/N_{\rm DF}=7$ for M_π^2 vs $1/\kappa$ and $\chi^2/N_{\rm DF}=20$ for f_π vs $1/\kappa$, yet go through the error bars of all the points. Recent work by Seibert [33] discusses potential problems with covariant fits of which this may be an example.

We continue to jackknife the entire fitting procedure and typically obtain statistical errors in the extrapolated results which are similar in size to the errors on the individual masses or amplitudes used in the fit. The systematic fitting error which we compute numerically (Sec. III C) roughly compensates for this underestimate—its largest contribution comes from analyses where we omit the heaviest meson and extrapolate from only the lightest two. Of course we cannot rule out the possibility that the problem plaguing this stage of the analysis stems from real physics—i.e., that the numerical data exhibit small violations of the leading-order chiral behavior, either because of the large values of the quark mass being used or because of problems with the quenched approximation itself [34]. A careful study of this issue will require larger lattices (allowing lighter quarks) and better statistics.

The results for f_K/f_π are plotted versus the lattice spacing in Fig. 6. Here the statistical and fitting errors have been added in quadrature. Note that we study the dimensionless ratio f_K/f_π (rather than f_K itself) as a

TABLE V. Light meson results at $\beta=5.7$, $16^3\times 25$ (point source). Fits were covariant, single-state, over $t=(6,9)$ for both correlators.

κ	$\chi^2/N_{\rm DF}$	aM	C_A	$af^{(0)}$	$af\times 10$
0.160	2.5	0.690(5)±0.011	0.289	0.634	1.83(10)±0.04
0.164	1.3	0.510(5)±0.006	0.272	0.556	1.51(9)±0.05
0.166	0.8	0.407(7)±0.006	0.263	0.515	1.35(9)±0.04
κ_c		$a\times m_\pi$[a]			1.12(10)±0.07[b]

κ_1	κ_2	$\chi^2/N_{\rm DF}$	aM	C_A	$af^{(0)}$	$af\times 10$
0.160	0.164	1.9	0.606(5)±0.007	0.281	0.595	1.67(9)±0.04
	0.166	1.6	0.562(5)±0.006	0.277	0.573	1.59(9)±0.04
	κ_c		0.489(4)±0.007			1.47(9)±0.04
0.164	κ_c		0.366(4)±0.006			1.33(9)±0.05
0.166	κ_c		0.306(5)±0.003			1.25(9)±0.06
κ_s	κ_c		$a\times m_K$[c]			1.38(14)±0.08[d]

[a] $\kappa_c=0.1690(1)\pm 0.0001$.
[b] $a^{-1}=1.2(1)\pm 0.1$ GeV.
[c] $\kappa_s=0.1623(12)\pm 0.0008$.
[d] $f_K/f_\pi=1.23(3)\pm 0.02$.

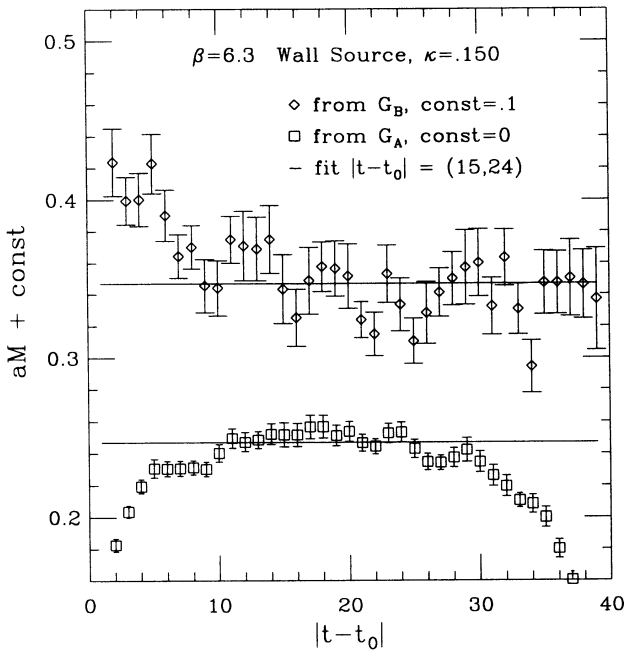

FIG. 2. The effective mass of the wall-source pion for $\kappa=0.150$ at $\beta=6.3$. The solid lines indicate the mass from the single-state fit, (3.10). So that both G_A and G_B masses may be shown simultaneously, the G_B mass is displaced upward by 0.1.

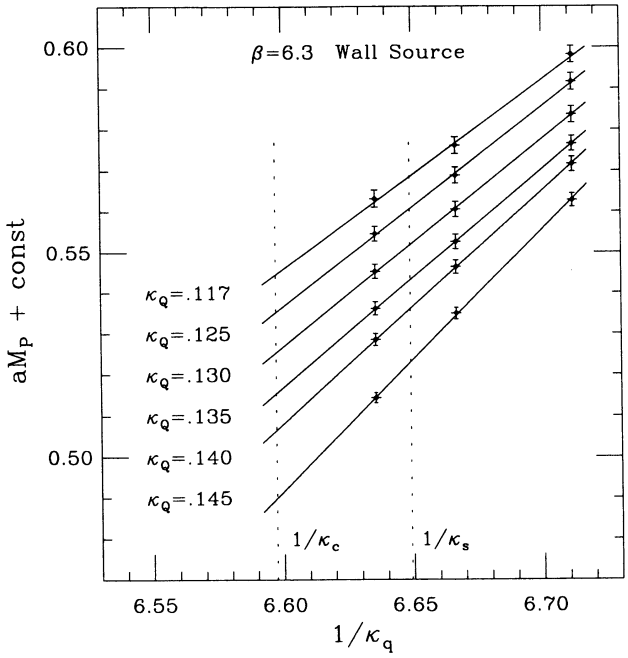

FIG. 4. Fits and extrapolations of the heavy-light masses for states with $M_P > 1$ GeV. The results have been offset by various amounts to improve the readability of the graph; the constants are $\kappa_Q=0.145$, $+0.130$; $\kappa_Q=0.140$, 0; $\kappa_Q=0.135$, -0.135; $\kappa_Q=0.130$, -0.275; $\kappa_Q=0.125$, -0.425; $\kappa_Q=0.117$, -0.700.

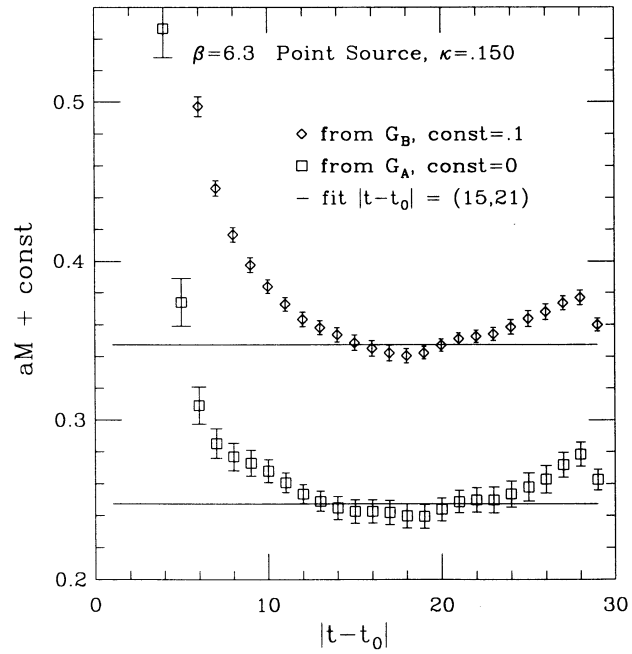

FIG. 3. The effective mass of the point-source pion for $\kappa=0.150$ at $\beta=6.3$. The solid lines indicate the mass from the single-state fit, (3.10).

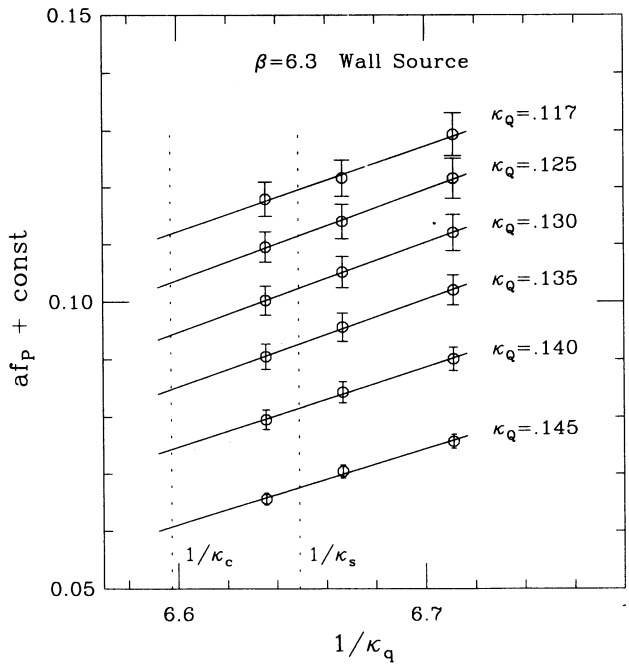

FIG. 5. Fits and extrapolations of the heavy-light decay constants for states with $M_P > 1$ GeV. The results have been offset by various amounts to improve the readability of the graph; the constants are $\kappa_Q=0.145$, 0; $\kappa_Q=0.140$, $+0.01$; $\kappa_Q=0.135$, $+0.02$; $\kappa_Q=0.130$, $+0.03$; $\kappa_Q=0.125$, $+0.04$; $\kappa_Q=0.117$, $+0.05$.

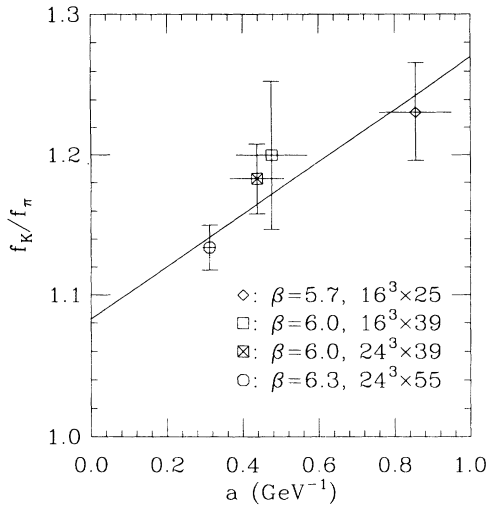

FIG. 6. Scaling study of (quenched) f_K/f_π.

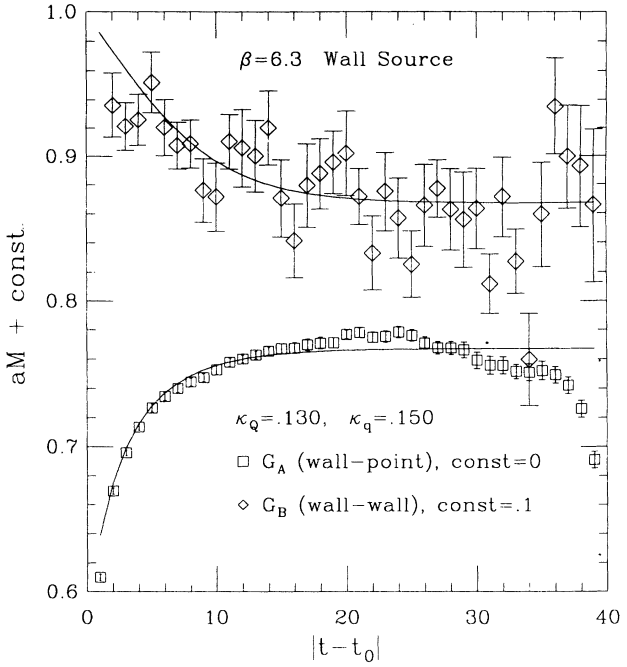

FIG. 7. The effective mass of the heavy-light wall-source correlators at β=6.3, κ_Q=0.130, and κ_q=0.150. The solid lines are the effective mass computed from the logarithmic derivative of the fitted function. The fitted interval was $|t-t_0|$=(3,18).

matter of convenience. There is no reduction in the statistical error since in dimensionful quantities we multiply the scale, which we determine from f_π, within the jackknife procedure. (That is to say, *all* of the decay constant computations are effectively made using a jackknifed "f/f_π" method.) From the linear fit shown in Fig. 6 we find the slope 0.19 ± 0.07 GeV^{-1} and the intercept $f_K/f_\pi(a=0)=1.08\pm0.03\pm0.08$. The first error is a measure of statistical and fitting errors; the second, systematic errors in the $a\to0$ extrapolation. We estimate the latter by repeating the fit using a quadratic, rather than linear, parametrization, and then symmetrizing the difference. This quenched result is 1.6σ less than the experimental value (1.22). It is interesting to note that the sign of the disagreement is in accord with sign of the difference between the chiral logs in the full and quenched theories [35].

C. Conventional heavy-light mesons

We focus here on the results at $\beta=6.3$. The three light quarks κ_L=0.149, 0.150, and 0.1507 are paired with the following "heavy" quarks: for wall sources κ_H=0.148, 0.145, 0.140, 0.135, 0.130, 0.125, and 0.117; for point sources κ_H=0.148, 0.145, 0.125, 0.110, and 0.100. As compared to the light mesons, the correlation functions, both wall and point, approach ground-state saturation more slowly. However, we found that the wall-source data were well approximated by the two-state function (3.11). These fits were made over a larger number of time slices which began much closer to the source. For quoted results we chose the interval $|t-t_0|$=(3,18) on each correlator, providing a total of 32 points in the fit. A sample of this method is shown in Fig. 7 for κ_H=0.130. The effective mass curve, computed from the logarithmic derivative of the fit function, provides the usual comparison of the fit to the data. In the alternate analyses from which we estimate fitting errors, we shift the intervals in either direction and also use single state fits at much larger time displacements. Results are reported in Tables VI–VIII. Note that we report the shifted mass aM', defined by Eq. (2.42), as well as the shift itself, $\Delta m_Q \equiv a\tilde{m}_2 - a\tilde{m}$, so that the bare lattice mass is easily obtained.

The analysis of the point-source heavy-light correlators was again worrisome due to the finite-time restriction, as can be seen from the effective mass plot, Fig. 8. Here the two-state function did not work well, and we have computed the single-state fits to these data as a check on the wall-source results. We cannot expect *a priori* that this analysis will produce a reasonable outcome, because we are forced to fit very close to the region where there are obvious, large boundary effects. In this respect, the agreement between the two methods (which is within the combined statistical and fitting errors estimated from the wall-source analysis) may be somewhat fortuitous. Note also that the statistical errors on the bare fitted amplitudes of the point-source analysis are actually smaller than the corresponding results from the wall sources for the *heavy-light* states (cf. κ_H=0.125 for the two cases). In the final analysis of physical quantities, however, we still obtain smaller statistical errors from the wall sources, primarily because of the smaller statistical error in the scale determination.

For each heavy quark κ_H, we extrapolate the correlator masses and decay constants linearly in $1/\kappa_L$ to the chiral and strange limits of the light quark. From the extrapolated values we recompute the amplitude ϕ_P which we analyze in conjunction with the static results for phenomenological predictions. The linear fit of f rather than ϕ is motivated by the results obtained [36] from the appli-

cation of chiral perturbation theory to mesons containing a single heavy quark [37,38]. In practice, however, the curvature is slight and it makes little difference which is used. The extrapolation points $1/\kappa_c$ and $1/\kappa_s$, computed in the light-meson analysis, are included in the jackknife. Since we neglect the inter-κ correlations in these fits, we again estimate a fitting error which includes analyses where extrapolations are made from the lightest two quarks. The fits and extrapolations of the heavy-light masses and decay constants are shown in Figs. 4 and 5, respectively.

D. Static results

For the static calculation, the use of smeared sources is necessary in order to obtain ground state dominance at sufficiently early times, and one would thus like to optimize the overlap of the source with the ground-state wave function of the heavy-light meson. In our simulations, however, the cube sources (Sec. III A) allow only a crude volume adjustment, and it is not clear *a priori* that any particular cube will sufficiently eliminate the contributions of higher states in both correlators. A search for an early plateau in the effective masses $M_A(t)$ and $M_B(t)$ or in the ratio of correlation functions G_A/G_B can lead to some judgment of the best smearing volume to use. However, for several reasons, this technique may not be entirely trustworthy and in practice difficult to implement. First, the effective mass of the smeared-point correlator, $M_A(t)$, need not be monotonic; this presents the possibility of short-range false plateaus, which are difficult to detect because the SNR is falling exponentially. Second, the location of the true plateaus in $M_A(t)$ and $M_B(t)$ need not coincide; thus the ratio G_A/G_B is difficult to interpret unambiguously. Finally, as based on some "best plateau" criterion, there is a noticeable variation in the optimum smearing volume as the light-quark mass is adjusted. Unless the source tuning procedure is sufficiently precise, different amounts of higher-state contamination at various light-quark masses will complicate the extrapolations to κ_c.

In this section we discuss the static-light analysis and present the results, first at $\beta=6.3$ and then at $\beta=6.0$. At

TABLE VI. Heavy-light, wall-source results at $\beta=6.3$. Fits were covariant, two-state, over $t=(3,18)$ for both correlators. aM' is the shifted mass defined by Eq. (2.42) and $\Delta m_Q \equiv a\tilde{m}_2 - a\tilde{m}$ is the value of the mass shift.

κ_H	κ_L	$\chi^2/N_{\rm DF}$	Δm_Q	aM'	C_A	$a^{3/2}\phi^{(0)}$	$a^{3/2}\phi\times 10$
0.148	0.149	0.8	0.000492	0.345(1)±0.002	0.252	0.160	0.403(5)±0.009
	0.150	0.9		0.314(1)±0.002	0.250	0.143	0.357(5)±0.008
	0.1507	1.2		0.290(1)±0.002	0.248	0.129	0.320(4)±0.006
	κ_s			0.300(2)±0.003			0.334(6)±0.008
	κ_c			0.263(2)±0.003			0.283(4)±0.009
0.145	0.149	0.8	0.00277	0.433(1)±0.002	0.259	0.191	0.495(8)±0.011
	0.150	0.9		0.405(1)±0.002	0.257	0.174	0.445(7)±0.011
	0.1507	1.1		0.384(1)±0.001	0.255	0.159	0.404(6)±0.009
	κ_s			0.392(2)±0.003			0.420(8)±0.011
	κ_c			0.360(1)±0.002			0.362(7)±0.012
0.140	0.149	1.0	0.0131	0.572(1)±0.002	0.270	0.223	0.602(15)±0.012
	0.150	1.0		0.546(1)±0.002	0.268	0.204	0.546(14)±0.013
	0.1507	1.2		0.528(1)±0.002	0.266	0.189	0.502(13)±0.013
	κ_s			0.535(2)±0.003			0.519(14)±0.013
	κ_c			0.507(1)±0.002			0.455(14)±0.015
0.135	0.149	1.2	0.0343	0.712(1)±0.002	0.281	0.245	0.688(22)±0.015
	0.150	1.2		0.688(1)±0.002	0.278	0.224	0.623(20)±0.015
	0.1507	1.3		0.671(1)±0.002	0.276	0.208	0.574(18)±0.016
	κ_s			0.678(2)±0.003			0.593(20)±0.015
	κ_c			0.651(2)±0.002			0.519(19)±0.019
0.130	0.149	1.4	0.0683	0.859(2)±0.002	0.291	0.260	0.756(31)±0.020
	0.150	1.3		0.836(1)±0.002	0.288	0.237	0.683(25)±0.016
	0.1507	1.5		0.820(1)±0.002	0.286	0.221	0.632(22)±0.018
	κ_s			0.826(2)±0.003			0.652(25)±0.017
	κ_c			0.801(2)±0.002			0.571(23)±0.021
0.125	0.149	1.6	0.117	1.017(2)±0.003	0.301	0.272	0.818(35)±0.026
	0.150	1.5		0.994(1)±0.002	0.298	0.246	0.734(31)±0.017
	0.1507	1.6		0.980(1)±0.003	0.296	0.231	0.684(26)±0.021
	κ_s			0.985(2)±0.003			0.704(29)±0.020
	κ_c			0.960(2)±0.002			0.617(27)±0.023
0.117	0.149	1.8	0.230	1.298(2)±0.003	0.316	0.284	0.898(42)±0.034
	0.150	1.7		1.276(2)±0.002	0.313	0.257	0.805(36)±0.023
	0.1507	1.9		1.263(2)±0.003	0.311	0.244	0.758(35)±0.028
	κ_s			1.268(2)±0.003			0.777(36)±0.026
	κ_c			1.245(2)±0.003			0.685(36)±0.027

TABLE VII. Heavy-light point-source results at $\beta=6.3$. Fits were covariant, single-state, over $G_A(17,23)$ and $G_B(18,23)$. See caption to Table VI.

κ_H	κ_L	$\chi^2/N_{\rm DF}$	Δm_Q	aM'	C_A	$a^{3/2}\phi^{(0)}$	$a^{3/2}\phi\times 10$
0.148	0.149	1.1	0.000514	0.351(2)±0.003	0.252	0.175	0.442(20)±0.016
	0.150	1.3		0.320(2)±0.003	0.250	0.160	0.401(20)±0.015
	0.1507	1.5		0.296(2)±0.002	0.248	0.147	0.365(19)±0.016
	κ_s			0.310(9)±0.007			0.385(28)±0.020
	κ_c			0.267(2)±0.004			0.327(21)±0.023
0.140	0.149	0.8	0.0133	0.578(2)±0.001	0.270	0.236	0.639(20)±0.015
	0.150	0.8		0.553(2)±0.001	0.268	0.216	0.580(21)±0.013
	0.1507	0.9		0.534(2)±0.001	0.266	0.203	0.540(21)±0.014
	κ_s			0.545(7)±0.005			0.563(29)±0.021
	κ_c			0.511(3)±0.002			0.488(23)±0.016
0.125	0.149	1.4	0.117	1.026(2)±0.002	0.301	0.287	0.864(22)±0.014
	0.150	1.6		1.004(2)±0.002	0.298	0.265	0.791(23)±0.014
	0.1507	1.7		0.987(3)±0.001	0.296	0.249	0.737(24)±0.014
	κ_s			0.997(7)±0.003			0.768(33)±0.024
	κ_c			0.966(4)±0.003			0.672(27)±0.021
0.110	0.149	2.6	0.371	1.588(12)±0.010	0.329	0.314	1.033(33)±0.030
	0.150	2.4		1.572(4)±0.005	0.326	0.283	0.925(31)±0.017
	0.1507	2.2		1.557(5)±0.004	0.324	0.265	0.860(35)±0.017
	κ_s			1.566(7)±0.004			0.899(46)±0.021
	κ_c			1.539(8)±0.006			0.765(43)±0.022
0.100	0.149	2.7	0.652	2.077(8)±0.009	0.347	0.316	1.097(41)±0.032
	0.150	2.6		2.058(5)±0.008	0.343	0.288	0.991(45)±0.037
	0.1507	2.5		2.045(7)±0.006	0.341	0.276	0.942(55)±0.027
	κ_s			2.053(8)±0.005			0.973(58)±0.026
	κ_c			2.028(9)±0.006			0.849(64)±0.037

$\beta=6.3$ we have better statistics, and the smearing techniques are more effective because the lattice is finer. We have used both wall and cube sources, the latter computed using a range of smearing volumes V_s. We choose our best results by demanding consistency among the different sources (and analysis methods) in order to minimize systematic errors from possible higher-state contamination as best we can. Our results at $\beta=6.0$, from cube sources only, are presented in comparison to other static results which have been published in the literature. At this lattice spacing, and with our statistics, we find that the finite time restriction (imposed by the exponentially falling SNR) and the limited effectiveness of the cube smearing together prevent us from making a convincing determination of the amplitude $\hat{\phi}$ [28]. Our results are smaller than previously reported [10], but there is still a strong dependence on how one chooses to analyze the data.

There is some similarity of our results at $\beta=6.0$ here with the results of Ref. [39] for difference size sources at a fixed fitting interval, but a crucial difference is that we do not believe there are any intrinsic problems with the cube-smearing technique. In principle, all sources must agree at large enough times. The issue, however, is that with limited statistics, a rapidly falling SNR, and only a few source sizes to choose from on this fairly coarse lattice, it can be difficult to go to large enough times. The data are then ambiguous, and guesswork will be involved in deciding the "optimal" available source and time interval to analyze the data.

1. $\beta=6.3$

We consider first a given smearing volume, e.g., $V_s=13^3$. The basic analysis procedure is analogous to that for the conventional method: we make a single-state, covariant fit to the two correlation functions over some range of time slices. The fitted parameters are the unrenormalized binding energy $a\mathcal{E}$ and the amplitudes $\hat{\xi}_A$ and $\hat{\xi}_B$ which enter into Eq. (2.6). This is repeated for several values of the light quark hopping parameter; we then make a linear fit of $\hat{\phi}$ vs $1/\kappa$ and extrapolate to $1/\kappa_c$ and $1/\kappa_s$, using the (jackknifed) parameters computed in the light-quark analysis. As in the previous cases, we neglect the inter-κ correlations. The effective masses for $V_s=13^3$, plotted against the mass obtained from a fit over the range $t=(9,16)$, are shown in Fig. 9.

Whereas the size of the cube source can be set to roughly match the size of the ground-state wave function, the size of the wall source is certainly too large. Thus higher-state contamination is expected to increase [28]. However, the wall has an advantage in terms of statistics (sources for both light and heavy quarks at every point on a time slice), and ultimately its performance must be evaluated empirically. Although there is a large admixture of excited states in the two-point functions (judging from the effective mass plots), we again obtain good fits for wall sources by using the two-state function over an early range of time slices. We use this method to extract the ground-state parameters needed to compute the static amplitude. The effective masses of the wall source,

static-light state, with $\kappa_q = 0.150$, are shown in Fig. 10 (see also Table IX). They are plotted against the curve computed from the logarithmic derivative of the fit function using the best-fit parameters as input.

A qualitative examination of the effective mass plots from the cube sources indicates that the optimum smearing volume is $V_s \sim 13^3 - 15^3$. Nevertheless, due to the caveats discussed above, our preference is to obtain consistent results over a range of V_s. In Fig. 11 we show the results of the raw decay amplitude (i.e., without perturbative renormalization constants) for several cube sizes. For each size, we show the dependence of the amplitude on the fitted time interval of the correlator G_A, while that for G_B has been held fixed at $t = (10, 16)$. We mark the fits which satisfy $\chi^2/N_{\rm DF} < 1$ with "×." The early-time fits clearly show systematic differences, but as the fit interval is moved further from the source, the results in the range $V_s \sim 13^3 - 17^3$ are in good agreement (both central values and size of errors) and are consistent with the wall-source results extracted from the two-state analysis [28]. If we instead use an early fit interval for G_B, fitting where the effective mass first appears to plateau, we find that these results are altered by at most 3%. (At $\beta = 6.0$, a similar change in the fit interval of the smeared-smeared correlator reveals a much larger discrepancy; see the discussion below.) We use the single-state fit over the later-time with the source $V_s = 15^3$ (presented in Table X) for our combined analysis from which we compute the B- and D-meson decay constants (Sec. IV E). The remaining systematic uncertainty associated with the source-type and fit interval is accounted for in the fitting error.

2. $\beta = 6.0$

At $\beta = 6.0$ we have poorer statistics and our results are less conclusive. Nevertheless, it is informative to compare them with those that have recently appeared in the

TABLE VIII. Heavy-light results at $\beta = 6.0$, $24^3 \times 39$. Fits were noncovariant, single-state, over $t = (10, 15)$ for both correlators. See caption to Table VI.

κ_Q	κ_q	Δm_Q	aM'	C_A	$a^{3/2}\phi^{(0)}$	$a^{3/2}\phi \times 10$
0.152	0.152	0.00116	0.488(8)±0.001	0.263	0.291	0.77(4)±0.01
	0.154		0.434(9)±0.001	0.258	0.254	0.66(4)±0.00
	0.155		0.406(9)±0.001	0.256	0.233	0.60(4)±0.00
	κ_s		0.399(19)±0.004			0.58(7)±0.01
	κ_c		0.354(8)±0.005			0.50(4)±0.01
0.148	0.152	0.00602	0.596(8)±0.001	0.272	0.353	0.96(5)±0.01
	0.154		0.546(9)±0.001	0.267	0.311	0.83(4)±0.01
	0.155		0.521(10)±0.001	0.265	0.288	0.76(4)±0.01
	κ_s		0.515(17)±0.004			0.75(7)±0.01
	κ_c		0.474(10)±0.004			0.64(4)±0.01
0.142	0.152	0.0240	0.757(8)±0.001	0.285	0.421	1.20(6)±0.01
	0.154		0.712(10)±0.001	0.280	0.373	1.04(6)±0.01
	0.155		0.689(11)±0.001	0.277	0.346	0.96(5)±0.01
	κ_s		0.683(14)±0.004			0.94(7)±0.01
	κ_c		0.646(12)±0.003			0.82(5)±0.01
0.135	0.152	0.0656	0.954(8)±0.001	0.299	0.475	1.42(7)±0.01
	0.154		0.912(10)±0.002	0.294	0.422	1.24(7)±0.01
	0.155		0.891(12)±0.002	0.291	0.392	1.14(6)±0.01
	κ_s		0.885(13)±0.004			1.12(8)±0.02
	κ_c		0.850(13)±0.003			0.97(6)±0.01
0.118	0.152	0.286	1.527(8)±0.003	0.332	0.558	1.85(9)±0.02
	0.154		1.488(11)±0.003	0.326	0.494	1.61(9)±0.02
	0.155		1.467(13)±0.004	0.323	0.457	1.48(9)±0.02
	κ_s		1.462(12)±0.004			1.45(9)±0.03
	κ_c		1.429(16)±0.003			1.25(10)±0.02
0.103	0.152	0.669	2.209(9)±0.004	0.358	0.610	2.18(12)±0.02
	0.154		2.171(12)±0.004	0.352	0.538	1.89(13)±0.03
	0.155		2.150(15)±0.005	0.348	0.496	1.73(14)±0.03
	κ_s		2.145(14)±0.004			1.70(12)±0.04
	κ_c		2.113(20)±0.004			1.45(16)±0.03
0.088	0.152	1.31	3.154(12)±0.005	0.382	0.657	2.51(17)±0.03
	0.154		3.116(16)±0.006	0.376	0.577	2.17(20)±0.03
	0.155		3.095(20)±0.006	0.372	0.530	1.97(21)±0.04
	κ_s		3.090(18)±0.005			1.93(18)±0.04
	κ_c		3.058(26)±0.005			1.64(25)±0.04

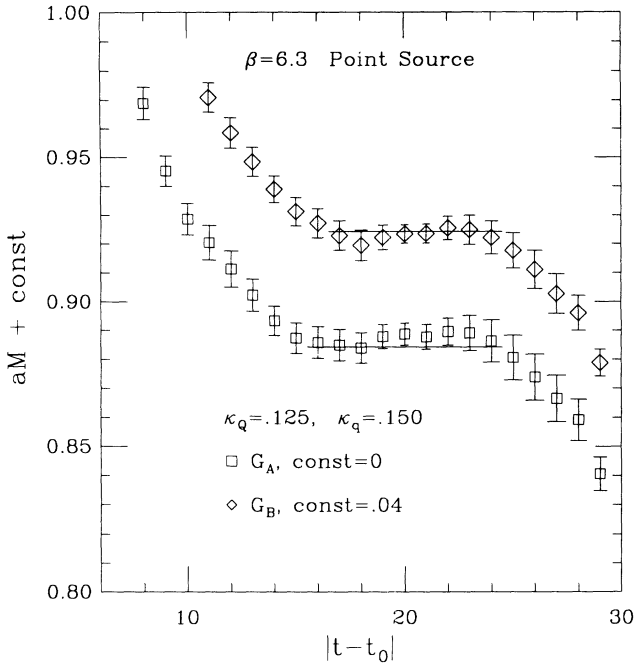

FIG. 8. The effective mass of the heavy-light point-source correlators at $\beta=6.3$, $\kappa_Q=0.125$, and $\kappa_q=0.150$. The solid lines indicate the fitted mass from the function (3.10) and the time intervals that were used.

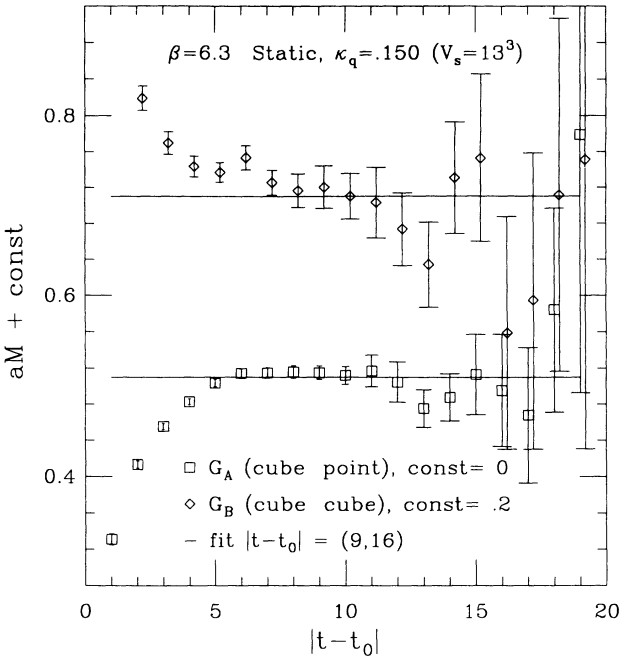

FIG. 9. The effective mass of the static correlators at $\beta=6.3$, $V_s=13^3$.

literature[2] [7,8,10,26]. Our aim here is to examine only the numerical aspects of the static calculation, independent of any questions of perturbative renormalization or choice of scale. To this end, we compile in Table XI results for the bare lattice quantity $\tilde{\phi}a^{3/2}\equiv\sqrt{2\kappa}\hat{\phi}^{(0)}a^{3/2}$, where

$$\hat{\phi}^{(0)}a^{3/2}\equiv\left[\frac{2\hat{\xi}_A^2}{\hat{\xi}_B}\right]^{1/2}.$$

In general we choose the light-quark hopping parameters $\kappa=0.154$ and $\kappa=0.155$; the European Lattice Collaboration (ELC) [8] used slightly different values; however, in each case we extrapolate the results linearly in $1/\kappa$ to the chiral limit (which we choose to be $\kappa_c=0.157$) so that a reliable comparison can be made. (We emphasize that all extrapolations to κ_c are ours, using our values for κ_c, a^{-1}, and the perturbative corrections to get $f_B^{\rm stat}$.) As a rough guide, the statistical error assigned to the extrapolated result has been taken from the lightest quark used in each case. To compute a physical value of f_B from the static calculation, the ELC [8] and Wuppertal [7] groups have used the perturbative renormalization $\hat{Z}_A=0.8$ and scale estimates of $a^{-1}=2.0$ and 2.3 GeV, respectively. In Ref. [10], we left open the choice of $\hat{Z}_A$ and used $a^{-1}=1.75$ GeV. These differences have been removed in computing $\tilde{\phi}$. From this "bare" result, we compute

$$f_B^{\rm stat}\equiv\hat{Z}_A C(a,M_B)\frac{\tilde{\phi}}{\sqrt{M_B}}\equiv C(a,M_B)\frac{\hat{\phi}}{\sqrt{M_B}},$$

with $a^{-1}=2.3$ GeV, $M_B=5.28$ GeV, and $\hat{Z}_A C(a,M_B)=0.70$; the latter obtained using $g^2=1.77$ (Sec. IV G).

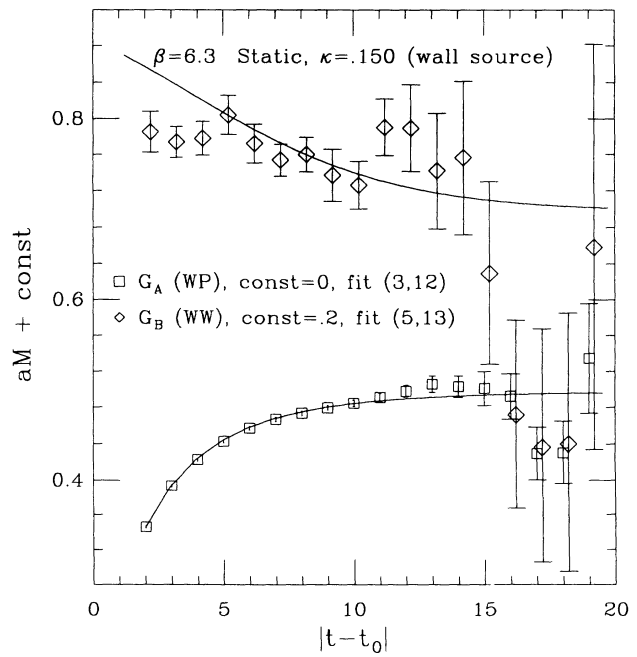

FIG. 10. Effective mass of the wall-source static correlators at $\beta=6.3$.

[2]Eichten *et al.* [40,9] have also reported results using smeared interpolating operators in the static limit. We do not include them here because the bare coupling was not the same (they used $\beta=6.1$, $\beta=5.9$, and $\beta=5.7$), and this makes an unambiguous comparison difficult. In addition, preliminary results from UKQCD were discussed in Ref. [41].

TABLE IX. Static-light, wall-source results at $\beta=6.3$. Fits were covariant, two-state, over $G_A(3,12)$ and $G_B(5,14)$.

κ	$\chi^2/N_{\rm DF}$	$a\mathcal{E}^{(0)}$	$\hat{C}_A/C(a,m)$	$a^{3/2}\hat{\phi}^{(0)}$	$a^{3/2}\hat{\phi}\times 10$
0.148	0.8	0.537(3)±0.004	0.395	0.290	1.15(7)±0.09
0.149	0.8	0.518(4)±0.004	0.392	0.268	1.05(6)±0.08
0.150	0.7	0.499(4)±0.004	0.388	0.246	0.96(6)±0.08
0.1507	0.7	0.487(6)±0.006	0.385	0.231	0.89(8)±0.13
κ_s		0.491(5)±0.006			0.92(7)±0.09
κ_c		0.470(6)±0.007			0.81(7)±0.11

The Wuppertal Collaboration has used gauge-covariant exponential wave functions as the smeared interpolating operators. In Table XI we denote their two-point functions which are analogous to our point-smeared (G_A) and smeared-smeared (G_B) by using our notation in quotes. In each of rows 1–3, the fitting technique is somewhat different, although in all cases an early interval has been used and the statistical errors are relatively small. Comparing the chiral extrapolations, the ELC and Wuppertal results agree at roughly the 10% level. The authors of Ref. [7] attribute the slightly lower ELC result to finite volume effects. There is a larger discrepancy ($\sim$30%) between our preliminary results in Ref. [10] (row 3) and those of the ELC group. ELC used the same smearing technique; however, they used a cube size $V_s=7^3$, whereas we chose $V_s=5^3$.

A sample of our updated results is presented in the lower two sections of Table XI. First, we recompute the amplitude at $V_s=5^3$ (row 4) to check the effect of changes in the analysis procedure—the difference is roughly within the statistical error (cf. rows 3 and 4). Next, at $V_s=7^3$, our central values are in very good agreement with those of the ELC calculation (cf. rows 1 and 5). Since the lattice sizes are different, this indicates that finite-volume errors are probably negligible at this level of precision. Continuing to $V_s=9^3$, however, we find that the amplitude again decreases—by approximately 20% when a similar (early) fitting interval is used. From our analysis, it is difficult to determine which of these is the "best" result based on some objective criterion such as the lowest $\chi^2/N_{\rm DF}$ of the fit.

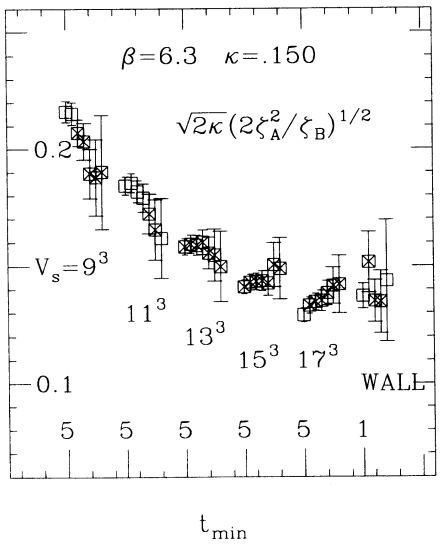

FIG. 11. The static-light amplitude at $\beta=6.3$, computed using different smearing sizes and fitting intervals. For each smearing function, the fit interval for G_B is held constant [$t=(10,16)$ for the cube sources, $t=(5,14)$ for the wall] and the interval for G_A is shifted in successive data points by one time slice, as indicated by the horizontal axis [$t=(t_{\rm min},t_{\rm min}+T)$, where $T=4$ for the cube sources, and $T=9$ for the wall source]. Fits which passed the criterion $\chi^2/N_{\rm DF}<1$ are marked with $\times$.

To illustrate the source of these differences, we show a sequence of effective mass plots in Fig. 12, using the light quark $\kappa=0.155$. In each plot the local masses of the smeared-smeared and smeared-point correlators, as well as the single mass from the coupled fit, are shown. (Because the number of lattices is small, we were not able to include the effects of correlations, and the values of $\chi^2/N_{\rm DF}$ which the fits produce are deceptively small.) As the smearing volume is increased from $V_s=5^3$ to 9^3, the effective masses appear to plateau earlier in the smeared-smeared correlator and later in the smeared point. This illustrates a problem with the cube source which was pointed out above; because of this we avoid using the ratio G_A/G_B in the analysis. In addition, there is some evidence that long-range (i.e., highly correlated in t) fluctuations are causing a misleading signal at $V_s=9^3$: the effective mass of G_B, a monotonically decreasing quantity, appears to rise slightly at the earliest time slices. The final analysis of these data thus requires a significant amount of judgment. We consider two approaches, both which seem fairly reasonable.

First, we repeat the procedure that was used at $\beta=6.3$. We use a later fit interval on the smeared-smeared correlator G_B and study the dependence of the amplitude on V_s and on the fit interval for G_A. These results, computed for the four values of the light quark hopping parameter, are shown in Fig. 13. At values of V_s where the amplitude is independent of $t_{\rm min}$, a plateau exists in the effective mass of the correlator G_A. By comparing the four plots, notice that using this particular "plateau criterion" will result in a different optimal smearing size for different light-quark masses—ranging from 5^3 at $\kappa_q=0.152$ to 9^3 at $\kappa_q=0.156$. Nevertheless, we again find (albeit within large statistical errors) that at large time displacements the results computed using different smearing volumes are in good agreement. As at $\beta=6.3$, we choose our best result from a later fit interval with a

TABLE X. Static-light, cube-source results ($V_s=15^3$) at $\beta=6.3$. Fits were covariant, single-state, over $t=(10,16)$ for both correlators.

κ	$\chi^2/N_{\rm DF}$	$a\mathcal{E}^{(0)}$	$\hat{C}_A/C(a,m)$	$a^{3/2}\hat{\phi}^{(0)}$	$a^{3/2}\hat{\phi}\times 10$
0.149	0.7	0.525(10)±0.008	0.392	0.294	1.15(6)±0.06
0.150	0.7	0.510(11)±0.009	0.388	0.275	1.07(6)±0.06
0.1507	0.6	0.499(11)±0.009	0.385	0.259	1.00(6)±0.05
κ_s		0.503(11)±0.009			1.02(6)±0.06
κ_c		0.486(12)±0.010			0.92(6)±0.06
$\hat{\phi}(\kappa_c)/\hat{\phi}(\kappa_s)=0.900(16)\pm0.018$					

large smearing function ($V_s=9^3$). An example of the outcome is provided in the final section of Table XI (i.e., row 7); we provide complete results in Table XII. Notice that at $\kappa=0.154$ this result is in good agreement with the corresponding one from $V_s=7^3$ (row 5, an earlier fitting interval): there is a plateau for the particular combination $V_s=7^3$ and $\kappa_q=0.154$. However, for $\kappa_q=0.155$ (a lighter quark), $V_s=7^3$ appears to be less optimal, and the difference between rows 5 and 7 becomes more pronounced. Because of this, there is an increase in the slope of the chiral extrapolation, which causes systematic differences to be magnified in $f_B^{\rm stat}$. This effect produces a significant amount of the difference between the result $f_B^{\rm stat}=237$ MeV in row 7 and, say, the ELC result $f_B^{\rm stat}=323$ MeV in row 1.

Alternatively, let us consider a different approach to the analysis, based on the effective-mass plot, Fig. 12(d). We assume that the early-time plateau in the smeared-smeared correlator (which is optimal for $V_s=9^3$) reflects the least contaminated projection onto the ground state and that the smeared-point correlator contains higher-state contributions which become small only at large times. Thus we fit $t=(2,9)$ for G_B and $t=(10,14)$ for G_A. Now, the fitted mass is primarily constrained by the smeared-smeared correlator and is significantly larger than that found in the first analysis described above [cf. Figs. 12(c) and 12(d)]. It does not appear to agree very well with the local masses of the smeared-point correlator, but our premise was that this channel contains substantial higher-state contributions and that, because of fluctuations and the overall signal loss, its effective-mass plateau is misleading. Thus, we compute the result given in the last row of Table XI, $f_B^{\rm stat}=364$ MeV.

From all of this, the first conclusion is that the bare lattice results coming from different simulations are in rather good agreement. As a final example of this point, note that the choice of fitting used to produce the latter (and larger) of the two results above is a similar approach as that used by the Wuppertal Collaboration, and the results agree well. The largest source of disagreement comes from the choice of analysis procedure. The fact that the disagreement exists implies that our data at $\beta=6.0$, and perhaps those of the other groups, are not very good. For the reasons discussed above, we have chosen the first of the two analyses as our best result. However, we cannot rule out a systematic error which is roughly given by the difference between the two. For the remainder of this paper, we will focus primarily on our results at $\beta=6.3$, which we find to be much less ambiguous.

E. Combined heavy-light analysis

In the final stage of the analysis, we combine the static and (large-am corrected) conventional results and analyze

TABLE XI. A comparison of static results at $\beta=6.0$. The results at specific κ values are taken directly from the papers, but all extrapolations to κ_c are ours, using our values for κ_c, a^{-1}, and the perturbative corrections to get $f_B^{\rm stat}$. We take the results from [7], rather than [26], since both $\kappa=0.154$ and $\kappa=0.155$ are included in the former. The results at $\kappa=0.154$ in [26] are completely consistent with those in [7].

Group (lattice)	Smearing	Fitting	$\tilde{\phi}a^{3/2}\equiv\sqrt{2\kappa}\hat{\phi}^{(0)}a^{3/2}$ $\kappa=0.154$	$\kappa=0.155$	Extrapolation in $1/\kappa$ Slope	$\tilde{\phi}(\kappa_c)a^{3/2}$	$f_B^{\rm stat}$ (MeV)
ELC [8]	Coul. gauge,	$G_B(4,9)$;	($\kappa=0.153$)	($\kappa=0.1545$)			
$10^2\times20\times36$	cube, $V_s=7^3$	$G_A/G_B(4,9)$	0.356(25)	0.337(24)	0.31	0.304(24)	323(26)
Wuppertal [7]	Gauge cov.,	"G_B" ($t\geq2$);	0.371(20)	0.359(20)	0.30	0.334(20)	355(21)
$12^3\times36$	exp. WF	"G_A" ($t\geq5$)					
Lattice '90 [10]	Landau gauge,	$G_B(5,10)$,	0.427(20)	0.416(20)	0.26	0.394(20)	419(21)
$24^3\times39$	cube, $V_s=5^3$	$G_A(5,10)$					
This work	Landau gauge,	Coupled fit,	0.419(18)	0.402(18)	0.41	0.369(18)	392(19)
$24^3\times39$	cube, $V_s=5^3$	$t=(5,10)$					
	$V_s=7^3$	$t=(4,9)$	0.337(10)	0.324(10)	0.31	0.299(10)	318(11)
	$V_s=9^3$	$t=(5,10)$	0.282(11)	0.268(12)	0.33	0.241(12)	256(13)
	$V_s=9^3$	$t=(8,13)$	0.315(36)	0.284(35)	0.74	0.223(35)	237(37)
	$V_s=9^3$	$G_B(2,9)$,	0.387(23)	0.372(23)	0.36	0.343(23)	364(24)
		$G_A(10,14)$					

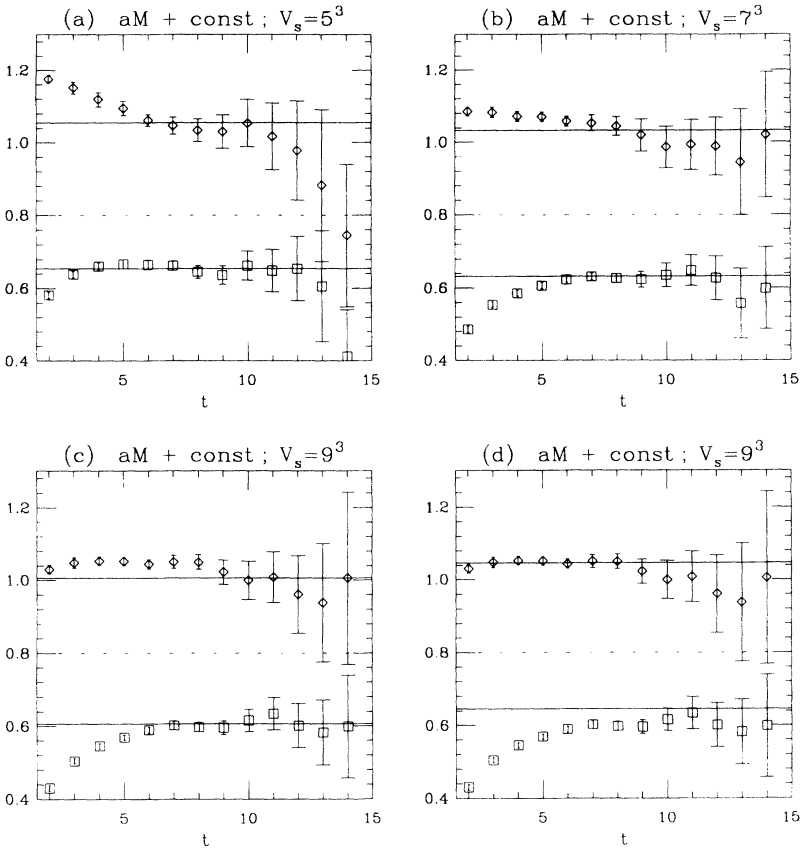

FIG. 12. Static-light effective masses at $\beta=6.0$, $24^3\times 39$, $\kappa_q=0.155$, for different smearing volumes. Diamonds: G_B (cube-cube), const $=+0.4$; squares: G_A (cube point), const $=0$. The solid lines indicate the mass from a coupled single-state fit. In plots (a)–(c) the fit interval on both correlators is $t=(5,10)$. In (d), the result for $V_s=9^3$ is repeated, showing the fitted mass from the ranges $G_B(2,9)$ and $G_A(10,14)$.

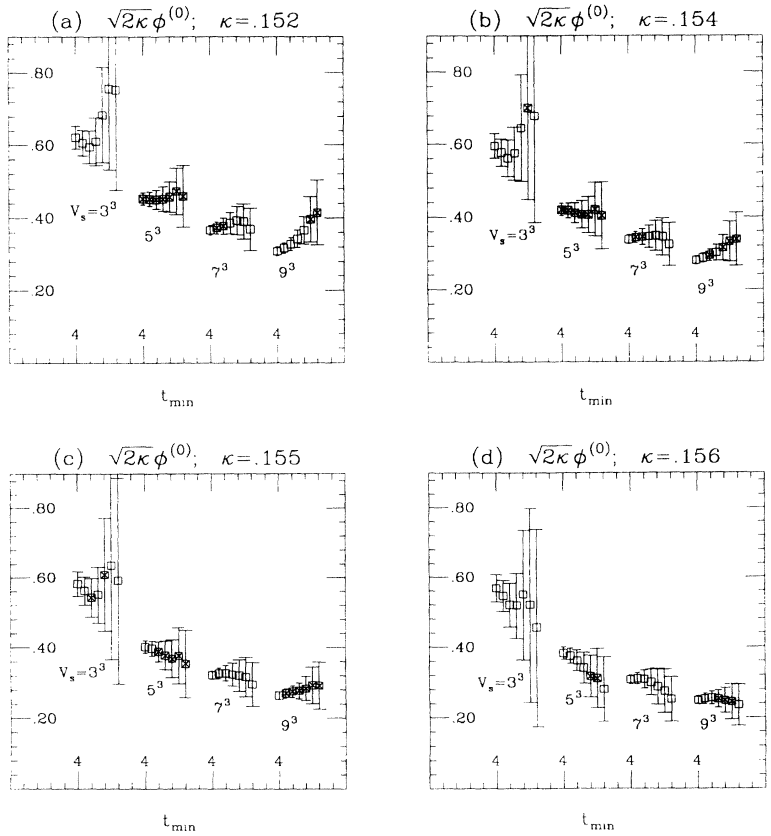

FIG. 13. A systematic study of the static-light amplitude at $\beta=6.0$ as a function of the light-quark mass, smearing size and fitting interval. In the coupled, single-state fit that produced each of the results, the fit intervals were $G_B(8,13)$ and $G_A(t_{\min},t_{\min}+4)$, where $t_{\min}$ is indicated on the horizontal axis and is shifted in successive data points by one time slice. The symbol $\times$ indicates $\chi^2/N_{\rm DF}<0.1$ (noncovariant).

TABLE XII. Static-light, cube-source ($V_s=9^3$) results at $\beta=6.0$. Fits were noncovariant, single-state, over $t=(8,13)$ for both correlators.

κ	$a\mathcal{E}^{(0)}$	$\hat{C}_A/C(a,m)$	$a^{3/2}\hat{\phi}^{(0)}$	$a^{3/2}\hat{\phi}\times 10$
0.152	0.68(2)±0.02	0.390	0.666	2.6(3)±0.2
0.154	0.63(2)±0.01	0.384	0.566	2.2(2)±0.1
0.155	0.61(2)±0.01	0.380	0.509	1.9(2)±0.1
κ_s	0.60(3)±0.01			1.9(2)±0.1
κ_c	0.57(3)±0.01			1.5(2)±0.1

them using the parametrization (2.38). The following is a summary of the essential steps leading to and including this stage of the analysis.

(1) Compute the static result $\hat{\phi}$ for $\kappa_q=\kappa_c$ and κ_s. The normalization $\hat{C}_A$ is given by (2.36) with the factor $C(a,m)$ removed. The light-quark extrapolations are described in Sec. IV D.

(2) Compute $\phi_P(\kappa_Q)$ and $M_P'(\kappa_Q)$, again for chiral and strange light quarks. C_A is given by (2.35) and M_P' is computed from the pole mass M_P according to (2.42). The light-quark extrapolations are described in Sec. IV C.

(3) Divide out the logarithmic factor $C(a,M_P')$ from the amplitude ϕ_P computed in step (2).

(4) Fit the amplitudes to a quadratic in $1/M_P'$. These fits are made using the jackknife estimation of the covariance matrix so that correlations among the heavy (and static) quarks are included and a meaningful $\chi^2/N_{\rm DF}$ is obtained (Sec. III C).

(5) Interpolate the fit to physical masses (e.g., $1/M_P'=1/M_B$) and multiply the logarithmic correction [e.g., $C(a,M_B)$] to obtain the physical amplitude.

In Fig. 14 we show the result from step (4) at $\beta=6.3$, where the light quark has been extrapolated to the chiral limit. The static point in all cases is taken from the source $V_s=15^3$, and the conventional points are from the wall-source results. From this analysis we find a smooth interpolation between the heavy lattice mesons and the static limit, as judged by a goodness-of-fit criterion: $\chi^2/N_{\rm DF}=1.9/3$ (heavy-chiral) and $\chi^2/N_{\rm DF}=3.4/3$ (heavy-strange). As the fit and extrapolation parameters are varied to estimate the fitting errors (Sec. III C), we generally find that the quality of the final fit is not severely altered.

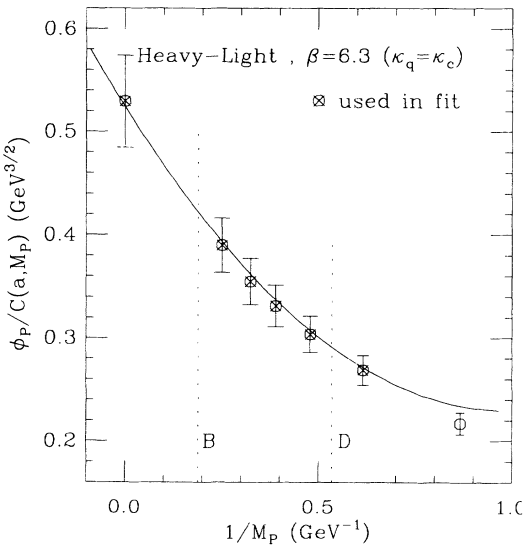

FIG. 14. The combined (conventional and static) analysis at $\beta=6.3$. The conventional points are from the wall-source results with the large-am corrections applied. The static point is from the cube source, $V_s=15^3$. The light quark has been extrapolated to the chiral limit. The (covariant) fit is quadratic in $1/M_P$, with $\chi^2/N_{\rm DF}=1.9/3$.

We obtain the deviations from the large-mass scaling behavior by extracting the first two coefficients of the fit function

$$F=c_0(1+c_1/M+c_2/M^2)\ . \tag{4.2}$$

We find

$$c_0=0.52(4)\ \text{GeV}^{3/2}\ ,$$

$$c_1=-1.14(15)\ \text{GeV}\ ,$$

$$\chi^2/N_{\rm DF}=1.9/3\ \text{(chiral light quark)}\ ,$$

and

$$c_0=0.58(3)\ \text{GeV}^{3/2}\ ,$$

$$c_1=-1.08(13)\ \text{GeV}\ ,$$

$$\chi^2/N_{\rm DF}=3.4/3\ \text{(strange light quark)}\ .$$

Interpolating these fits, using the experimentally measured masses, and taking $M_{B_s}=M_B+(M_{D_s}-M_D)$, we obtain the decay constants

$$f_B=187(10)\pm 12\ \text{MeV}\ ,$$

$$f_D=208(9)\pm 11\ \text{MeV}\ ,$$

$$f_{B_s}=207(9)\pm 10\ \text{MeV}\ ,$$

$$f_{D_s}=230(7)\pm 10\ \text{MeV}\ .$$

The first error is statistical, obtained by a full jackknife of the procedure outlined above (Sec. III C); the second is the systematic fitting error, computed as described in Sec. III D.

F. Large-am errors

We consider now the systematic error associated with the large-am corrections introduced in Secs. II D and II E. In Fig. 15 we plot the heavy-strange results, both

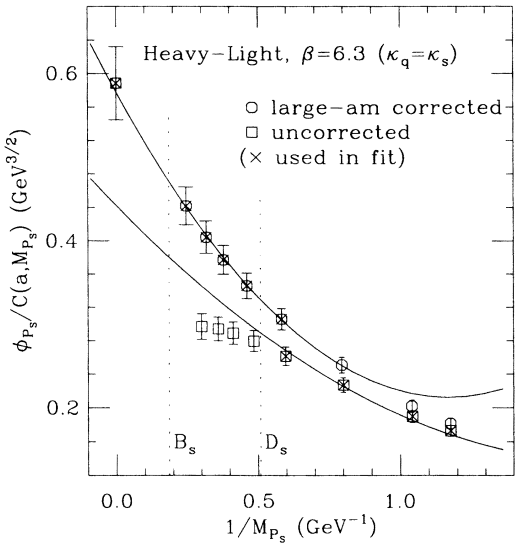

FIG. 15. The heavy-light amplitude, with $\kappa_q=\kappa_s$. The circles are the results with large-*am* corrections included. The squares are the corresponding results with those corrections removed. The fit to the latter is an attempt to smoothly interpolate between the static limit and the conventional results in a region where $O(am)$ errors might, *a priori,* have been negligible. (See text, Sec. IV F).

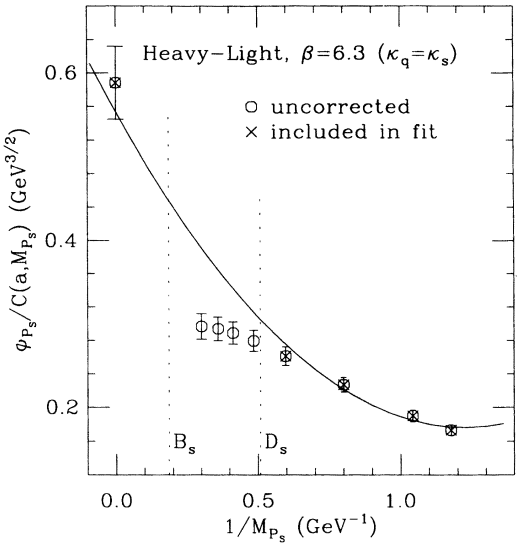

FIG. 16. The heavy-light amplitude, again with $\kappa_q=\kappa_s$ and without including the large-*am* corrections. Here we show the effect of using an uncorrelated fit to the data, to be compared with the corresponding result in Fig. 15.

corrected and uncorrected [the latter are computed by removing the factors of $e^{a\tilde{m}}$ in Eqs. (2.35) and (2.36), and eliminating the mass shift (2.42)]. Using the uncorrected results, we make the following two analyses. First, we fit the set of points corresponding to the same values of κ_Q that were used in the analysis above, including the static. Noting that in this case ϕ flattens out at a value well below the static result, we would not expect a good fit. Indeed, we find $\chi^2/N_{\rm DF}=28/3$ (heavy-chiral) and $\chi^2/N_{\rm DF}=32/3$ (heavy-strange). However, given that aM_P is ~ 1 for the heaviest mesons used, it is more legitimate to argue that when excluding the corrections one should throw out the largest masses and attempt to interpolate between the static limit and an intermediate-mass regime where lattice errors might, *a priori,* be small enough. This has been the traditional approach; an example of it is shown in Fig. 15, where we eliminate from the fit uncorrected points with $a\tilde{m}>0.3$. Note that we still find a discrepancy between the static and conventional results which is characterized by poor fits: we find $\chi^2/N_{\rm DF}=16/2$ (heavy-chiral) and $\chi^2/N_{\rm DF}=16/2$ (heavy-strange). Either $O(am)$ errors are still too large, or else the conventional points are too far from the heavy-quark scaling regime to model the data using (2.38). As discussed further in the following section, we are unable to obtain good fits, even after allowing changes in the analysis parameters to accommodate fitting and scale systematics. Furthermore, we emphasize here the importance of using the covariant fit in arriving at the above conclusions: since the conventional points are highly correlated, the trend in the data is significant, and only the covariant fits are able to take this into account. By contrast, we show in Fig. 16 the corresponding uncorrelated fit, where the discrepancy between the two methods appears to be much less pronounced. Thus, without the large-*am* corrections applied to the Wilson quark, there remains a significant discrepancy between the static and conventional methods—even at $\beta=6.3$, using results where lattice errors should be the smallest.

We now attempt to characterize the systematic errors associated with large *am*. Since the factor e^{am} acts at leading order, its full effect is, in principle, an overestimate of the systematic error which remains in the corrected amplitude when the heavy quark is nonrelativistic. A better approach is to consider the correction at $O(1/M_P)$ directly. We discuss three methods below.

The first approach is to reanalyze the data with the leading-order correction in place, but without making the shift in M_P, given by (2.42). The difference between a quantity computed from this analysis and that from the fully corrected one gives some idea of the size of the subleading large-*am* corrections. Although the mass shift is significant at the largest masses, in both analyses the fit is constrained by the static point and by the lighter mesons, upon which the shift has a small effect. Consequently, the error estimates turn out to be quite small—for the amplitudes f_B, f_{B_s}, f_D, and f_{D_s} they range between 2–3 %. (With or without the mass shift we obtain good fits, i.e., $\chi^2/N_{\rm DF}\simeq 1$.)

A second approach is to try to examine explicitly the error caused by the suppression of the $\sigma\cdot\mathbf{B}$ term. The shift in M_P adjusts the heavy-quark mass to the kinetic value $\tilde{m}_2(\kappa_Q)$. Using this as the definition of the quark mass, let us write the true amplitude as

$$\phi_{\rm true}\simeq\hat{\phi}\left[1+\frac{X_{\rm kin}}{2\tilde{m}_2}+\frac{X_{\sigma\cdot\mathbf{B}}}{2\tilde{m}_2}\right]+O\left[\frac{1}{\tilde{m}_2^2}\right]. \tag{4.3}$$

Our lattice result is given instead by

$$\phi_{\rm latt} \simeq \hat{\phi}\left[1+\frac{X_{\rm kin}}{2\tilde{m}_2}+\frac{X_{\sigma\cdot B}}{2\tilde{m}_3}\right]+O\left[\frac{1}{M^2}\right], \qquad (4.4)$$

where the difference between $\tilde{m}_2$ and $\tilde{m}_3$ is discussed in Sec. II E. In principle, we could fit the lattice data to the form (4.4), determine the parameters $\hat{\phi}$, $X_{\rm kin}$, and $X_{\sigma\cdot B}$, and reconstruct the true amplitude from (4.3). A more stable approach, numerically, would be to choose three heavy mass points (including, perhaps, the static point) and *solve* for the three unknown parameters. The inherent systematic errors could then be estimated by varying the choice of the three points. Unfortunately, when we apply this analysis here, we find that the current data are just not precise enough: Estimates of the difference between $\phi_{\rm latt}$ and $\phi_{\rm true}$ at the B meson mass vary between approximately 5% and 40%, depending on the three points chosen and on whether the masses $\tilde{m}_2$ and $\tilde{m}_3$ are adjusted to take into account the difference between the heavy quark mass and heavy-light meson mass (which should be a higher-order effect).

It is easy to understand why the above method fails with the current data. From Fig. 14, one sees that the dependence of ϕ_P on $1/M_P$ is quite linear for the heavier masses which lead up to the static point. It will therefore be hard to pull out the coefficient $X_{\sigma\cdot B}$, which is responsible for nonlinearities in (4.4) and for the difference between (4.4) and (4.3).

Since the first method is rather *ad hoc,* and since the second may be giving indications of considerably larger errors, we have implemented a third approach. This approach, while indirect, has the advantage that it estimates the combined systematic errors due to all identified problems that affect the large-am points: the perturbative mismatch with the static computation (Sec. II D), the procedure for treating the logarithmic corrections (Sec. II F), as well as the difference between $\tilde{m}_2$ and $\tilde{m}_3$. The idea is to eliminate all heavy quark points with $a\tilde{m} > 0.17$ (i.e., all but our lightest three heavy quarks—this corresponds to eliminating all mesons with mass $aM > 0.36$ for a chiral light quark) and to fit the remaining points in conjunction with the static value. We take the difference between the results of these fits and the previously discussed central values as our estimate of the large-am systematic error. From Fig. 15 one sees that the fit to the large-am corrected points comes quite close even to the light-mass points that were not included in the fit. Thus, it should be no surprise that we get quite small error estimates if we use the same fitting form (4.2) on the light-mass points alone. However, one may argue that, without the heavy-mass points, we have no direct evidence for the basically linear behavior of ϕ_P vs $1/M_P$ in the region of the B. We therefore chose, as a possible smooth interpolation between the light-mass points and the static limit, a quartic fit in $1/M_P$ with the coefficient of the linear term set equal to 0. (Since there are four remaining parameters and only four points to fit, we actually just solve for the parameters.) The result is shown in Fig. 17. This gives a considerably larger deviation from the central values, and we take this deviation as a conservative estimate of the combined large-am error. The results of this analysis are given in Table XIV.

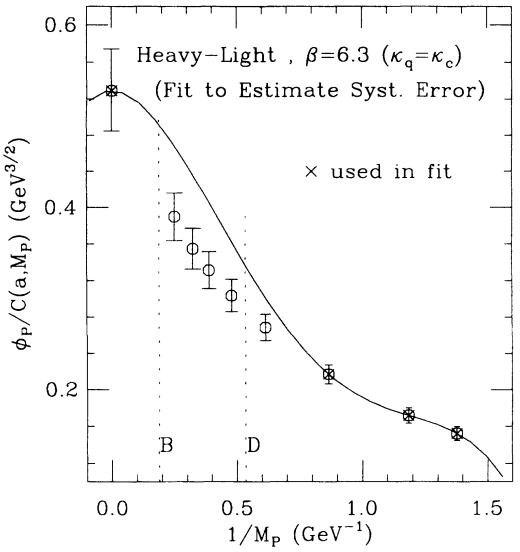

FIG. 17. The heavy-light amplitude, with $\kappa_q = \kappa_c$, fit as described in the text in order to estimate a bound on various systematic errors.

G. Scale errors and other systematics

To study scale errors, one can in principle consider two approaches. The first and preferable way is to repeat the calculation at a variety of different lattice spacings, thereby computing "physical" results as a function of a [e.g., $f(a)$]. Let us refer to any deviation from scaling behavior [$f(a)$=const] as a "pure" scale violation; we computed this error to be $\simeq 6\%$ for f_K at $\beta=6.3$ (Sec. IV B). Alternatively, at a given lattice spacing, one can simply use several different methods to determine a^{-1} and compare the results. The scale error computed this way is less informative because it includes other systematic effects (such as quenching) in an unknown way. In either case, there are two issues which we wish to consider: (1) the connection between scale errors and large-am effects, and (2) the estimation of a systematic error in physical amplitudes.

Combining results[3] at $\beta=6.3$ and $\beta=6.0$, we first examine the scaling behavior of the heavy-light amplitude both with the large-am corrections (Fig. 18) and without them (Fig. 19). Assuming that the corrections remove most of the large-am systematics, there may be some evidence for scaling violations in Fig. 18, but the differences between $\beta=6.0$ and $\beta=6.3$ are not much larger than the statistical errors. In the uncorrected case the difference

[3]The analysis procedure at $\beta=6.0$, $24^3\times 39$ (8 configurations), was analogous to that at $\beta=6.3$, with the following exceptions: No fits were covariant, and individual configurations were time-reversal averaged before jackknifing. In addition, for the scaling comparisons depicted in Figs. 18 and 19, we have not (at $\beta=6.0$) included the scale $a_{f_\pi}^{-1}$ in the jackknife analysis. This results in a smaller statistical error—the one that is typically reported in lattice simulations.

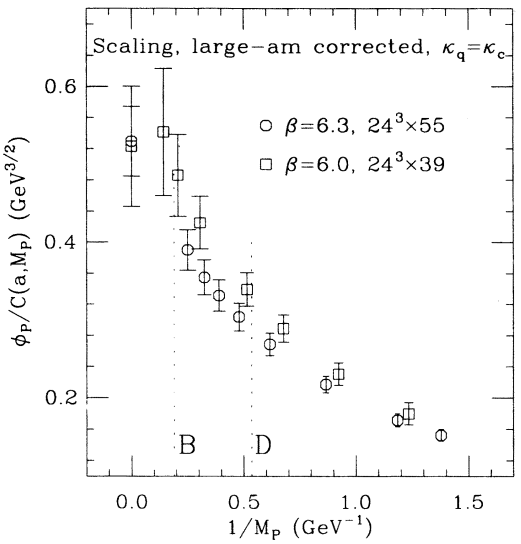

FIG. 18. Scaling comparison ($\beta=6.3$ and $\beta=6.0$) of the heavy-light amplitude, computed with the large-*am* corrections.

between the results at the two couplings is smaller in general. Note, however, that there is a difference between the trends of the two simulations at the highest masses. At $\beta=6.0$, the onset of the downward slope in the uncorrected amplitude is evident, presumably due to the "$e^{-aM_P/2}$," behavior discussed in Sec. II C. At $\beta=6.3$, the heavy-mass data are still rising, but with decreasing slope—presumably a smaller-*am* manifestation of the same effect. Our conclusion is that the high-mass $\beta=6.0$ data suffer from additional suppression relative to the $\beta=6.3$ data, and that the apparent agreement between the two couplings is accidental, indicating a cancellation between the large-*am* errors and true scaling violations. However, other interpretations are clearly possible. Because of the limitations of our method and the quality of the data, it is difficult to disentangle specific effects such as this in an unambiguous way. Thus, the scaling behavior between $\beta=6.3$ and $\beta=6.0$ cannot be used to choose between the corrected and uncorrected conventional method in the regime $am \lesssim 1$; nor can a quantitative estimate of pure scaling violations be made for these data.

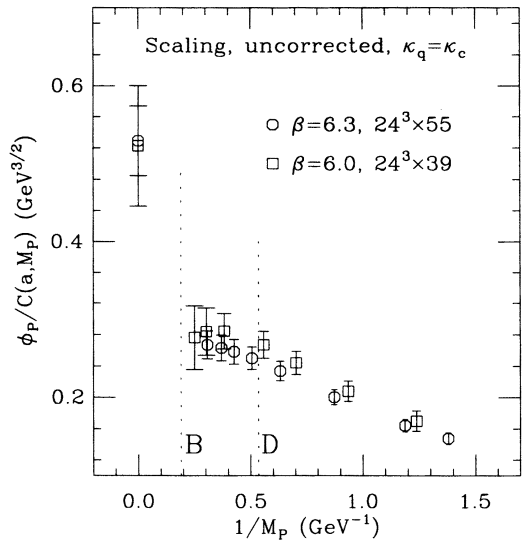

FIG. 19. Scaling comparison ($\beta=6.3$ and $\beta=6.0$) of the heavy-light amplitude, computed without large-*am* corrections.

Let us use the results at $\beta=6.3$ and consider the scale error in terms of an uncertainty in a^{-1}. If we choose f_K to set the scale, the outcome can be more or less predicted from Fig. 6. The difference between the ratio $f_K/f_\pi(\beta=6.3)$ and f_K/f_π(phys) is about 7%; this essentially translates directly to other quantities, although there are additional effects in this case since we fit ϕ_P vs $1/M_P$ in physical dimensions. Recomputing the full analysis using $a^{-1}(f_K)$, we find a systematic shift of $\sim 8\%$ in the decay constants of the D and B mesons.

Of course, we may consider a variety of other ways to choose the scale—the string tension, the nucleon mass, the rho mass, etc. In principle, the most conservative bound will be obtained using $a_{M_\rho}^{-1}$, since here the discrepancy with $a_{f_\pi}^{-1}$ is typically quite large. In this simulation we have not computed the vector mesons; however, high-statistics studies of the string tension [42] and the quenched hadron spectrum [43] allow us to make an estimate of the difference in these scales at $\beta=6.3$. To do this, we first interpolate the string tension results of [42] to $\beta=6.17$. We choose this coupling because it is the weakest one used in the spectrum calculation of [43], from which we obtain aM_ρ. Using $\sqrt{\sigma}=440$ MeV and the physical value of M_ρ, we compute the relative scale error $(a_{M_\rho}^{-1}-a_\sigma^{-1})/a_\sigma^{-1}\simeq 0.08$. This we expect to bound the corresponding error at $\beta=6.3$. Therefore, we interpolate the string tension results to $\beta=6.3$ and make the scale assignment $a_{M_\rho}^{-1}=1.08a_\sigma^{-1}$. (At $\beta=6.3$ we find $a_\sigma^{-1}=3.18$ GeV, similar to the scale we obtain from f_π, and thus $a_{M_\rho}^{-1}=3.44$ GeV.) Note that the scale error obtained this way is slightly larger than the one determined from f_K; we choose the larger value in order to make a conservative error estimate.

We show the results of the analysis using this scale in Table XIII. From the top half of the table (large-*am* corrected) we compute the systematic scale error quoted with our final results. All other aspects of this analysis were unchanged from that which produced our central values. The lower half of the table contains the results computed without the large-*am* corrections and restricted to $a\tilde{m}\leq 0.3$, as described in the previous section. The point here is that despite the change to the scale $a_{M_\rho}^{-1}$, there still remains a discrepancy between the conventional and static methods, which is indicated by the large value of $\chi^2/N_{\rm DF}$ for the fit.

Since we use f_π to set the scale for our central values, any uncertainty in the choice of coupling used in the perturbative renormalization constants Z_A and $\hat{Z}_A$ will have only a small effect in the final results for the heavy-light decay constants. That is to say, in the conventional amplitude $f\sqrt{M}$, a change in g^2 will have no effect since a jackknifed f/f_π method is used—the factors of Z_A cancel. There will be residual effects due to the change in the

TABLE XIII. Interpolations from ϕ vs $1/M$ with shifted scales ($\beta=6.3$).

Large am	a^{-1} (GeV)	κ_q	$\chi^2/N_{\rm DF}$	f_{cq} (MeV)	f_{bq} (MeV)
Corrected	3.44	κ_c	1.9/3	220(7)	202(8)
		κ_s	3.5/3	248(6)	229(8)
Uncorrected	3.44	κ_c	18/2	204(5)	168(6)
		κ_s	17/2	224(4)	189(6)

ratio $\hat{Z}_A/Z_A$ and the scale which normalizes the masses M_P to be used in the final fit of ϕ vs $1/M_P$. Our central values are obtained using the "boosted" coupling $g_V^2(\tilde{q})$ derived from the heavy-quark potential; the momentum $\tilde{q}$ is defined as the average $\ln(q^2)$ of the tadpole graph, $\tilde{q}=2.58/a$ [21]. This produces the values

$$\beta=5.7,\ g_V^2\simeq 1.95\ ;$$
$$6.0,\quad 1.77\ ;$$
$$6.3,\quad 1.62\ .$$

By repeating the analysis using the bare coupling ($g^2=6/\beta$), we find changes in the heavy-light decay constants of $\lesssim 3\%$. However, based on the studies presented in [21], the bare coupling is, in any case, a poor choice of expansion parameter; we expect this to be an overestimate of the uncertainty in the final results. Since there exists reasonable motivation for using the boosted coupling, and since the residual effect of changes in the coupling is so small, we consider this uncertainty to be subsumed in our general estimate of scale errors and do not include it as a separate source of systematic error.

We expect finite-volume errors to be negligible compared to the other errors, even though our 24^3 lattice has a volume of only $\sim(1.5\ \text{fm})^3$. This is because we work only with pseudoscalar meson states at zero three-momentum, which are quite insensitive to volumes of this size. For example, in the calculation [44] of B_K with staggered fermions, no significant difference was found between the results for 16^3 and 24^3 lattices at $\beta=6.0$; the 16^3 lattice has almost the identical physical volume as our $\beta=6.3$ lattice. Similarly, Tables III and IV show no difference, at the level of our statistics, for f_K/f_π or a^{-1} between our 16^3 and 24^3 lattices at $\beta=6.0$. Note that finite size effects on the heavy-light pseudoscalar states should be even less than for light-light states, since the former are somewhat smaller in size. Of course, the size of the finite-volume effects should be checked explicitly for the current computation; that work is in progress.

Our results for the decay constants and bounds for various systematic errors are summarized in Table XIV.

TABLE XIV. Decay constants and systematic error estimates.

Meson	f (MeV)	Fitting and extrapolation	Scale ($a_{M_\rho}^{-1}$)	Large am
B	187(10)	±12	±15	±32
B_s	207(9)	±10	±22	±32
D	208(9)	±11	±12	±33
D_s	230(7)	±10	±18	±28

In Table XV we present the jackknifed ratios and similar estimates of systematics. For final results, we add the fitting and/or extrapolation and large am errors in quadrature. These two errors are estimated through similar numerical procedures which are essentially independent of each other. We list the scale error separately. Thus, we find

$$f_B=187(10)\pm 34\pm 15\ \text{MeV}\ ,$$
$$f_D=208(9)\pm 35\pm 12\ \text{MeV}\ ,$$
$$f_{B_s}=207(9)\pm 34\pm 22\ \text{MeV}\ ,$$
$$f_{D_s}=230(7)\pm 30\pm 18\ \text{MeV}\ ,$$

where the first error (in parentheses) is statistical, and the second two are systematic, representing respectively the large-am plus fitting errors, and the scale errors.

We now briefly recall the experimental status regarding the measurement of these quantities. For f_D there only exists an upper bound at present, $f_D<290$ MeV (90% C.L.) [45]. Recently an important first step in the experimental determination of f_{D_s} was made, yielding $f_{D_s}=232\pm 45\pm 20\pm 48$ MeV [46]. For now the errors in this measurement are too large for it to have an impact on lattice calculations of f_{D_s}; improved measurements are eagerly awaited. Once a precise experimental determination of f_D or f_{D_s}—or for that matter any one of the four heavy-light decay constants—becomes available, then lattice results on the ratios of the f's (see Table XV) could prove useful in pinning down the values of the others, since the errors on the ratios are rather small ($<5\%$).

V. CONCLUSION

We have computed the heavy-light decay constants f_B, f_{B_s}, f_D, and f_{D_s} in the quenched approximation at $\beta=6.3$. The results have been summarized above; in addition we present the results for the jackknifed ratios in Table XV. Included in these calculations, we have computed the ratio f_K/f_π, extrapolated to the limit of zero

TABLE XV. Jackknifed ratios.

Ratios	Central	Fitting and extrapolation	Scale ($a_{M_\rho}^{-1}$)	Large am
f_B/f_D	0.90(3)	±0.02	±0.02	±0.01
f_{B_s}/f_{D_s}	0.90(2)	±0.02	±0.02	±0.02
f_B/f_{B_s}	0.90(2)	±0.03	±0.02	±0.02
f_D/f_{D_s}	0.90(2)	±0.02	±0.02	±0.03

lattice spacing. Here we find, for the quenched theory, $f_K/f_\pi = 1.08 \pm 0.03 \pm 0.08$. There are several important aspects of this work which warrant some additional concluding remarks.

First, the reliability of the static method must be considered independently of any comparison to the conventional calculation (and, preferably, independently of issues of scale and renormalization). Early results for $f_B^{\rm stat}$ were significantly larger than those reported here, as emphasized in Sec. IV D. The most likely source of such discrepancy is that various computational techniques (i.e., sources, fitting, etc.) are sensitive to different amounts of higher-state contamination in the correlation functions. Unlike the pion correlator, the static-light channel suffers from an exponentially falling SNR. To boost the ground-state signal in early time slices, various smearing techniques have been used, both in this work and elsewhere. However, higher-state errors remain a difficult issue, because the fundamental problem of noise at large times is not eliminated by the smearing. To minimize the error, we have studied the dependence of the amplitude on the size of the cube source and on the range of fitted time slices. Physical results must of course be independent of the source, which is only used as a tool for the lattice calculation. And, while it is not guaranteed that more than one cube size will be satisfactory, it is equally possible that none will be: a cube is a poor approximation to the ground-state wave function to begin with, and excited-state contamination may never be sufficiently reduced. Consistency of the results over some range of sources provides a reliable check that this is in fact not the case.

At $\beta = 6.3$, we see agreement between the static results from different smearing volumes, around some size which is presumably characteristic of the ground-state wave function, and from the wall source, where a different (two-state) fit was used over an early range of time slices. The "best" cube size, based on the earliest plateau in the effective masses, depends on the light-quark mass. For our final results, we have used larger smearing volumes (which in this sense are optimal for the lightest quarks) and later fitting intervals, where the overall dependence on cube size is minimized. However, the results from earlier fitting intervals are not very different, and we included the variations in our estimate of the systematic error from fitting. We report our final results from this simulation.

At $\beta = 6.0$, our sample is smaller and the cube sources cannot be adjusted as precisely. Apparently for these reasons, the $\beta = 6.0$ static results are considerably more ambiguous. The results from a range of different smearing volumes only agree when we use a later fitting interval. (The "best" cube size depends strongly on the light quark mass.) We therefore tend to prefer such later fitting intervals, and this preference results in a significantly smaller value of $f_B^{\rm stat}$ (237 MeV) than has previously been reported at $\beta = 6.0$. Nevertheless, we find it difficult to rule out alternate analyses, in which the correlation functions are fit at considerably earlier times. Such analyses of our data can produce a value for $f_B^{\rm stat}$ as large as 364 MeV.

At $\beta = 6.3$, we use an interpolation between the static and conventional heavy-light results in order to estimate the corrections to the asymptotic scaling law (1.2). We find large coefficients [e.g., $c_1 = -1.14(15)$ GeV], and thus the correction to the amplitude ϕ_P is significant for the B meson ($\simeq 20\%$) and large for the D ($\simeq 45\%$). In fact, the D meson is much better simulated by using the conventional lattice method, as long as suitable adjustments are made for Wilson fermions at quark masses near the scale of the inverse lattice spacing (i.e., $am \lesssim 1$). This statement is justified, not by a comparison of our results to experiment (the errors in the experimental measurement of f_{D_s} [46] are still too large to help us much in this regard), but rather by the observation that only when large-am corrections are included in the calculation do we find that the large-mass extrapolation of the heavy-light amplitude agrees with the static calculation. In practical terms, we characterize this agreement (or lack thereof, if the leading order correction is omitted) by the $\chi^2/N_{\rm DF}$ of the correlated fit to the combined set of results.

The systematic error which remains uncorrected in the conventional calculation, and the extent to which it affects the interpolation to the physical amplitudes, is unfortunately difficult to estimate. We have argued that, in terms of a nonrelativistic expansion, the leading-order correction is essential but that the next-to-leading one is difficult, but perhaps not impossible, with good data, to include in a systematic way, because the kinetic and $\boldsymbol{\sigma}\cdot\mathbf{B}$ interactions are, for large am, incorrectly normalized with respect to each other in the standard Wilson action. In Sec. IV F we used three methods to estimate the error incurred in the decay constants, and the results were rather dissimilar. The first method simply demonstrates that the large-am correction based on the kinetic term of the nonrelativistic expansion (i.e., the shift in M_P) has a small effect on the final correlated fit. The second is an attempt to address directly the unwanted lattice artifact—the suppression of the $\boldsymbol{\sigma}\cdot\mathbf{B}$ interaction. Unfortunately, the present data are just not precise enough to support this type of analysis. The third approach estimates this large-am error [and, concurrently, the errors induced by the perturbative mismatch with the static computation (Sec. II D) and the procedure for treating the logarithmic corrections (Sec. II F)] by dropping all quark masses with $a\tilde{m} > 0.17$ and reanalyzing the remaining points under conservative assumptions. The results are reported in Table XIV under "large am."

Finally, let us return to the conventional results at heavy masses and the issue of the leading-order correction, the factor of e^{am} in the Wilson quark normalization. We note that in the literature, results exist [47] which are in contrast to what we have found here—namely, that this correction must be included in order to eliminate the large discrepancy between the static and conventional decay constants. The difference between our results and those of Ref. [47], where similar methods were used, appears not to be in the static point (both calculations were at weaker couplings, $\beta = 6.2$–$\beta = 6.4$, and the static results are in better agreement than at $\beta = 6.0$) but rather in

the conventional amplitude. In short, they see the elimination of the old discrepancy at these weaker couplings without the e^{am} corrections, but we do not. However, as opposed to the analysis of Ref. [47], we have consistently used covariant fits throughout so that the effect of correlations in the data are not missed when attempting to study numerically the interpolation between the static and heavy-quark regimes. A conclusive resolution of this discrepancy will clearly require improved source techniques (and longer lattices) so that any question of the integrity of the raw lattice measurements is first addressed.

Questions such as this, however, only pertain to the calculation of a precise result with the conventional method; the result thereby obtained is not necessarily an accurate one, as we have already emphasized. To remove the ambiguity in the decay constant at $O(1/M)$ requires an improved action (so that the normalization of $\sigma \cdot \mathbf{B}$ relative to the kinetic energy term is corrected) or better data in the large mass region (so that the difference between $1/m_2$ and $1/m_3$ can be extracted cleanly), or both. Control of these effects, in turn, would facilitate the study of other key systematics, such as scale violations. Work along these lines is in progress.

Noted added. After this paper was submitted for publication, a new experimental measurement of f_{D_s} was announced by the CLEO Collaboration: $f_{D_s}=344\pm37\pm52\pm42$ MeV [48]. Although the central value of this result is noticeably high compared to our results (and those of other lattice groups), it is premature to draw any conclusions due to the size of the errors.

ACKNOWLEDGMENTS

We thank A. Kronfeld, P. Lepage, P. Mackenzie, and S. Sharpe for very useful discussions, and C. M. Heard for help with the computing. The computations were performed at the San Diego Supercomputer Center and the National Energy Research Supercomputer Center; we thank both centers for their generous help. The authors C.B., J.L., and A.S. were supported in part by the U.S. Department of Energy under Grant Nos. DE2FG02-91ER40628, DE-FG06-91ER40614, and DE-AC02-76CH0016, respectively.

[1] E. Eichten, in *Field Theory on the Lattice,* Proceedings of the International Symposium, Seillac, France, 1987, edited by A. Billoire *et al.* [Nucl. Phys. B (Proc. Suppl.) **4**, 170 (1988)].

[2] M. B. Voloshin and M. A. Shifman, Yad. Fiz. **45**, 463 (1987) [Sov. J. Nucl. Phys. **45**, 292 (1987)]; H. D. Politzer and M. B. Wise, Phys. Lett. B **206**, 681 (1988); N. Isgur and M. B. Wise, *ibid.* **232**, 113 (1989); **237**, 527 (1990); H. Georgi, *ibid.* **240**, 447 (1990).

[3] For a review of this and related problems, see C. Bernard, in *From Action to Answers,* edited by T. DeGrand and D. Toussaint (World Scientific, Singapore, 1990); C. Bernard and A. Soni, in *Lattice Approach to Electroweak Matrix Elements in Quantum Fields on the Computer,* edited by M. Creutz (World Scientific, Singapore, 1993); C. Sachrajda, in *Lattice '92,* Proceedings of the International Symposium, Amsterdam, The Netherlands, 1992, edited by J. Smit and P. van Baal [Nucl. Phys. B (Proc. Suppl.) **30**, 20 (1993)].

[4] C. Bernard, T. Draper, G. Hockney, and A. Soni, Phys. Rev. D **38**, 3540 (1988).

[5] M. B. Gavela, L. Maiani, G. Martinelli, O. Pène, and S. Petrarca, Phys. Lett. B **206**, 113 (1988).

[6] For similar work restricted to D mesons, see T. A. DeGrand and R. D. Loft, Phys. Rev. D **38**, 954 (1988).

[7] C. Alexandrou, F. Jegerlehner, S. Güsken, K. Schilling, and R. Sommer, Phys. Lett. B **256**, 60 (1991).

[8] C. Allton, C. Sachrajda, V. Lubicz, L. Maiani, and G. Martinelli, Nucl. Phys. **B349**, 598 (1991).

[9] E. Eichten, G. Hockney, and H. B. Thacker, in *Lattice '90,* Proceedings of the International Symposium, Tallahassee, Florida, 1990, edited by U. M. Heller, A. D. Kennedy, and S. Sanielevici [Nucl. Phys. B. (Proc. Suppl.) **20**, 500 (1990)].

[10] C. Bernard, J. Labrenz, and A. Soni, in *Lattice '90* [9], p. 488.

[11] C. Bernard, J. Labrenz, and A. Soni, in *Lattice '92* [3], p. 465.

[12] E. Eichten and B. Hill, Phys. Lett. B **240**, 193 (1990).

[13] M. B. Wise, in *Particle Physics—The Factory Era,* Proceedings of the Lake Louise Winter Institute, Lake Louise, Canada, 1991, edited by B. A. Campbell *et al.* (World Scientific, Singapore, 1991).

[14] Ph. Boucaud, Lin Chyi Lung, and O. Pène, Phys. Rev. D **40**, 1529 (1989); **41**, 3541(E) (1990).

[15] E. Eichten and B. Hill, Phys. Lett. B **234**, 511 (1990).

[16] Ph. Boucaud, J. P. Leroy, J. Micheli, O. Pène, and G. C. Rossi, Phys. Rev. D **47**, 1206 (1993).

[17] B. Meyer and C. Smith, Phys. Lett. **123B**, 62 (1983); G. Martinelli and Y. C. Zhang, *ibid.* **123B**, 443 (1983); R. Groot, J. Hoek, and J. Smit, Nucl. Phys. **B237**, 111 (1984).

[18] P. Mackenzie, in *Lattice '92* [3], p. 35; in *The Fermilab Meeting,* Proceedings of the Annual Meeting of the Division of Particles and Fields of the APS, Batavia, Illinois, 1992, edited by C. Albright *et al.* (World Scientific, Singapore, 1993).

[19] A. S. Kronfeld, in *Lattice '92* [3], p. 445.

[20] P. Lepage, in *Lattice '91,* Proceedings of the International Symposium, Tsukuba, Japan, 1991, edited by M. Fukugita *et al.* [Nucl. Phys. B (Proc. Suppl.) **26**, 45 (1992)].

[21] G. Peter Lepage and Paul B. Mackenzie, Report No. FERMILAB-PUB-19/355-T (9/92), 1992 (unpublished).

[22] B. A. Thacker and G. Peter Lepage, Phys. Rev. D **43**, 196 (1991).

[23] The introduction of smeared sources and early numerical studies can be found in A. Billoire, E. Marinari, and G. Parisi, Phys. Lett. **162B**, 160 (1985); P. Bacilieri *et al.*, Nucl. Phys. **B317**, 509 (1989). Smeared sources for the static approximation were first used in [25].

[24] The wall source technique was first used with staggered

fermions. See R. Gupta, G. Guralnik, G. W. Kilcup, and S. R. Sharpe, Phys. Rev. D **43**, 2003 (1991).
[25] E. Eichten, G. Hockney, and H. B. Thacker, in *Lattice '89*, Proceedings of the International Symposium, Capri, Italy, 1989, edited by R. Petronzio *et al.* [Nucl. Phys. B (Proc. Suppl.) **17**, 529 (1990)].
[26] C. Alexandrou, S. Güsken, F. Jegerlehner, K. Schilling, and R. Sommer, CERN Report No. CERN-TH 6692/92, 1992 (unpublished); in *Lattice '92* [3], p. 453.
[27] G. P. Lepage, in *From Action to Answers* [3].
[28] C. Bernard, C. M. Heard, J. Labrenz, and A. Soni, in *Lattice '91* [20], p. 384.
[29] E. Eichten, in *Lattice '91* [20], p. 391.
[30] D. Toussaint, in *From Action to Answers* [3].
[31] W. Press, B. Flannery, S. Teukolsky, and W. Vetterling, *Numerical Recipes: The Art of Scientific Computing* (Cambridge University Press, Cambridge, England, 1986).
[32] See, for example, R. Gupta, C. F. Baillie, R. G. Brickner, G. W. Kilcup, A. Patel, and S. R. Sharpe, Phys. Rev. D **44**, 3272 (1991).
[33] D. Seibert, CERN Report No. CERN-TH.6892/93, hep-lat/9305014 (unpublished).
[34] C. Bernard and M. Golterman, in *Lattice '92* [3], p. 217; S. Sharpe, *ibid.*, p. 213.
[35] C. Bernard and M. Golterman, in *Lattice '91* [20], p. 360; Phys. Rev. D **46**, 853 (1992).
[36] B. Grinstein, E. Jenkins, A. Manohar, M. J. Savage, and M. Wise, Nucl. Phys. **B380**, 369 (1992).
[37] M. B. Wise, Phys. Rev. D **45**, 2188 (1992).
[38] G. Burdman and J. Donoghue, Phys. Lett. B **280**, 287 (1992).
[39] S. Hashimoto and Y. Saeki, Mod. Phys. Lett. A **7**, 387 (1992).
[40] A. Duncan, E. Eichten, A. X. El-Khadra, J. M. Flynn, B. R. Hill, and H. Thacker, in *Lattice '92* [3], p. 433.
[41] UKQCD Collaboration, J. Simone, in *Lattice '92* [3], p. 461.
[42] G. S. Bali and K. Schilling, Phys. Rev. D **47**, 661 (1993).
[43] F. Butler, H. Chen, J. Sexton, A. Vaccarino, and D. Weingarten, Phys. Rev. Lett. **70**, 2849 (1993).
[44] G. W. Kilcup, S. R. Sharpe, R. Gupta, and A. Patel, Phys. Rev. Lett. **64**, 25 (1990).
[45] J. Adler *et al.*, Phys. Rev. Lett. **60**, 1375 (1988).
[46] WA75 Collaboration, S. Aoki *et al.*, Prog. Theor. Phys. **89**, 131 (1993).
[47] A. Abada *et al.*, Nucl. Phys. **B376**, 172 (1992).
[48] D. Acosta *et al.*, CLNS Report No. CLNS 93/1238 (unpublished).